Escola de Camins
Escola Tècnica Superior d'Enginyeria de Camins, Canals i Ports
UPC BARCELONATECH

Calibrating and Validating a Coupled Physical and Biokinetic Model of Denitrification in the Hyporheic Zone of Streams

TREBALL FINAL DE GRAU

Treball realitzat per:
Irene Benito Lázaro

Dirigit per:
Prof. Maarten Willem Saaltink (UPC)
Prof. Stanley B. Grant (University of California, Irvine)

Grau en:
Enginyeria Civil

Barcelona, 13 de juny de 2017

Departament d'enginyeria civil i ambiental

Acknowledgements

I would first like to thank the Balsells Mobility Fellowship, for giving me the opportunity of fulfilling a dream. Carrying out research in the U.S. and experiencing the engineering world in this country would not have been possible without this help. Balsells Mobility Fellowship has, furthermore, allowed me to broaden my knowledge about the American culture and meet fascinating people through these six months at the University of California, Irvine.

Secondly, I would like to thank my tutor at University of California, Irvine, Stanley B. Grant, for teaching me all the essentials of hyporheic exchange and the insights of research, and my tutor at UPC, Maarten W. Staaltink for helping me whenever was necessary.

I would also like to thank Morvarid Azizian, from University of California, Irvine, for providing unconditional support during the course of my thesis.

Finally, I must express my infinite gratitude to my parents for their belief in me that gives me courage to pursue all my dreams and ambitions.

This thesis is dedicated to Norberto Lázaro. Thank you for being eternally proud of me. You will always be loved.

Abstract

Human activities have increased the input of bioavailable nitrogen into the rivers and streams across the world. This has caused harmful effects on ecosystem and human health, so that U.S. National Academy of Engineering has identified restoring balance to the nitrogen cycle as one of the 14 Grand Challenges facing engineers in the 21st Century. Biogeochemical processing of nitrogen in the hyporheic zone of streams, on the other hand, is thought to be an effective pathway for removing excess nitrate in these systems. In this thesis, I used a previously published method, called PASS model, to calculate direct denitrification velocity of nitrate ($v_{f,Dw}$), which is defined as the ratio of the flux of nitrogen gas generated by direct denitrification and in-stream concentration of nitrate. I aimed to calibrate PASS model parameters and validate its results with a well-known set of data that was collected as part of the second lotic intersite nitrogen experiment (LINX II) across 72 streams in the United States. Altogether, I calibrated four fundamental parameters of the PASS model, including hyporheic exchange flux coefficient (a), rate constant of dissolved organic carbon mineralization ($R_{min,0}$), nitrification rate constant (k_{NI}), and denitrification rate coefficient (κ). I interpreted the results of the calibration by using Multiple Linear Regression (MLR) and Bootstrap techniques. At the end I cross-validated the results from the calibrated PASS model with the LINXII data, in terms of two indicating uptake velocities, namely oxygen and nitrate uptake velocities and I performed a model goodness analysis reporting Nash-Sutcliff efficiency for each set of the model validation results.

Contents

Table of Figures

Notations

a	hyporheic exchange flux coefficient (-)
AR	aerobic respiration
BIC	Bayesian information criterion
CH_2O	formaldehyde representing dissolved organic carbon
CI	confidence interval
CO_2	carbon dioxide (mol m^{-3} s^{-1})
$C_{NH_4^+}$	concentration of ammonium (mol m^{-3} s^{-1})
$C_{NO_3^-}$	concentration of nitrate (mol m^{-3} s^{-1})
C_{O_2}	concentration of oxygen (mol m^{-3} s^{-1})
$C_{S\text{-}NH_4^+}$	in-stream concentration of ammonium (mol m^{-3} s^{-1})
$C_{S\text{-}NO_3^-}$	in-stream concentration of nitrate (mol m^{-3} s^{-1})
$C_{S\text{-}O_2}$	in-stream concentration of oxygen (mol m^{-3} s^{-1})
DN	denitrification
DOC	dissolved organic carbon
d_S	depth of stream (m)
d_{50}	median grain size diameter of the streambed (mm)
ER	ecosystem respiration (mol m^{-2} s^{-1})
$E(\tau)$	probability density function form of the hyporheic zone residence time distribution (s^{-1})
F_N	fraction of nitrate
g	gravitational constant (m s^{-2})
GPP	gross primary production (mol m^{-2} s^{-1})
H	height of ripples (m)
κ	denitrification rate coefficient (-)
k_{NI}	nitrification rate constant (m^3 mol^{-1} s^{-1})
$K_{NO_3^-}^{sat}$	half-saturation constant for denitrification (mol m^{-3})
$K_{O_2}^{inh}$	oxygen inhibition of denitrification (mol m^{-3})
$K_{O_2}^{sat}$	half-saturation constant for aerobic respiration (mol m^{-3})
λ	wavelength of a ripple (m)
LINX II	second lotic intersite nitrogen experiment
m	empirical parameter (-)
MLR	multiple linear regression
MTL	mass transfer limited

NI	nitrification
NSE	Nash-Sutcliff efficiency
PASS	pumping and streamline segregation model
POC	particulate organic carbon
Q	stream discharge ($m^3\ s^{-1}$)
q_H	hyporheic exchange flux ($m\ s^{-1}$)
$q_{H,0}$	characteristic hyporheic exchange flux ($m\ s^{-1}$)
q_U	horizontal component of ambient groundwater flux ($m\ s^{-1}$)
q_V	vertical component of ambient groundwater flux ($m\ s^{-1}$)
R_{AR}	rate of aerobic respiration ($mol\ m^{-3}\ s^{-1}$)
R_{DN}	rate of denitrification ($mol\ m^{-3}\ s^{-1}$)
R_{min}	rate of mineralization of sediment organic matter ($mol\ m^{-3}\ s^{-1}$)
$R_{min,0}$	site-specific mineralization rate at the sediment-water interface ($mol\ m^{-3}\ s^{-1}$)
R_{NI}	rate of nitrification ($mol\ m^{-3}\ s^{-1}$)
RMSE	root mean squared error
s_0	streambed slope
SEMS	structural equation models
τ	travel time through the hyporheic zone (s)
τ_R	respiration timescale (s)
τ_0	characteristic time for organic carbon mineralization (s)
τ_{50}	median residence time (s)
θ	porosity (-)
$U_{N_2,Dw}$	flux of nitrogen gas out of the streambed by direct denitrification of stream nitrate ($mol\ m^{-2}\ s^{-1}$)
$U_{N_2,Dn}$	flux of nitrogen gas out of the streambed by coupled denitrification-denitrification ($mol\ m^{-2}\ s^{-1}$)
$U_{NO_3^-}$	flux of nitrate out of the sediment ($mol\ m^{-2}\ s^{-1}$)
v_f	total nitrate uptake velocity ($m\ s^{-1}$)
$v_{f,Dw}$	direct denitrification ($m\ s^{-1}$)
$v_{f,Dn}$	coupled nitrification-denitrification ($m\ s^{-1}$)
$v_{f,MTL}$	nitrate uptake under mass transfer limited conditions ($m\ s^{-1}$)
v_{f,O_2}^{field}	uptake velocity of oxygen reported by LINX II study ($m\ s^{-1}$)
v_{f,O_2}^{PASS}	uptake velocity of oxygen from PASS model ($m\ s^{-1}$)
v_{fden}^{field}	direct denitrification uptake velocity reported by LINX II study ($m\ s^{-1}$)
$v_{f,DW}^{PASS}$	direct denitrification uptake velocity from PASS model ($m\ s^{-1}$)
VIF	variance inflation factor
z_0	characteristic sediment where organic carbon mineralization takes place (m)

1. Introduction

Over the past century humans more than doubled the input of bioavailable nitrogen to terrestrial landscapes, primarily in the form of fertilizer for agricultural applications [*Kaushal et al.,* 2008; *Lassaletta et al*., 2009]. Much of this excess nitrogen finds its way to streams and rivers through point and non-point sources of pollution, including return flows from irrigated agriculture, runoff from confined animal feeding operations, septic tank leachate, and partially treated municipal wastewater discharges, to name a few [*Yates*, 1985; *Jongbloed and Lenis*, 1998; *Carey and Migliaccio*, 2009]. The environmental impacts of this nitrogen pollution are myriad, including eutrophication of inland and coastal waters [*Ryther and Dunstan*, 1971; *Smith et al*., 1999; *Cook et al*., 2006], ocean acidification [*Keeling et al*., 2010; *Cai et al.,* 2011, *Chan et al.,* 2016], and greenhouse gas generation [*Kroeze et al.,* 1999; *Beaulieu et al*., 2011; *Steffen et al*. 2015; *Marzadri et al*., 2017]. Thousands of stream, river, lake, groundwater, and coastal sites in the U.S. are classified as impaired for nitrogen by the U.S. Environmental Protection Agency [*Schot and van der Wal*, 1992, *Hancock*, 2002; U.S. E.P.A, 2017]. The U.S. National Academy of Engineering has identified restoring balance to the nitrogen cycle as one of the 14 Grand Challenges facing engineers in the 21st Century [U.S. NAE, 2017].

The environmental and human health consequences of nitrogen pollution are mitigated, to some degree, by in-stream treatment; i.e., the natural ability of streams and rivers to remove nitrate by direct denitrification (microbial reduction of stream nitrate to harmless dinitrogen gas) and ammonium by coupled nitrification-denitrification (the microbial

oxidation of ammonium to nitrate followed by its subsequent reduction to dinitrogen gas) [*Grathwohl et al*., 2013]. On the other hand, incomplete denitrification of nitrate in streams and rivers can lead to the emission of nitrous oxide, a potent greenhouse gas [*Beaulieu et al*., 2011; *Marzardri et al*., 2017]. Thus, relative to nitrogen pollution, streams and rivers perform both an ecosystem service (removal of in-stream nitrogen by direct denitrification and coupled nitrification-denitrification) and ecosystem disservice (generation of nitrous oxide through incomplete denitrification).

Biogeochemical processing of nitrogen in streams is thought to occur mostly in the hyporheic zone [*Zarnetske et al*., 2012; *Harvey et al*., 2013], defined as the portion of the streambed where hydrologic flow paths begin and end in the stream [*Gooseff,* 2010; *Boano et al*. 2014]. Because denitrification requires anoxic conditions, its onset in the hyporheic zone is controlled by a balance between the removal of oxygen by aerobic respiration (respiration time scale, τ_R) and the residence time of water in the hyporheic zone (median residence time, τ_{50}), sometimes expressed by the dimensionless Damköhler number $\left(Da = \tau_{50}/\tau_R\right)$ (*Zarnetske et al*. [2011, 2012]; *Harvey et al*. [2013]; *Gomez-Velez et al*. [2015]; *Azizian et al*. [2017]). A trade-off may arise in which nitrate uptake by the hyporheic zone is reduced when the Damköhler number is either too large or too small. For large values ($Da \gg 1$) redox conditions in the hyporheic zone are favorable for denitrification but the slow movement of solutes limits the mass of nitrate that can be removed (mass transfer-limited conditions). For small values ($Da \ll 1$) nitrate passes through the hyporheic zone largely unreacted because redox conditions are unfavorable for denitrification (reaction-limited conditions). Optimal nitrate uptake may

occur when the transport and respiration timescales are roughly equal; i.e., when $Da \approx 1$ [*Harvey et al*., 2013; *Gomez et al*., 2015; *Herzog et al*., 2015].

An unsolved challenge is how the concepts described above can be scaled up to entire stream networks. Such information is needed for a number of practical end points, including assessment of the contribution of streams and rivers to global nitrogen budgets [*Kiel and Cardenas,* 2014; *Gomez-Velez et al*., 2015] and global nitrous oxide production [*Marzadri et al*., 2014, 2017], as well as better management of point and non-point source nitrogen pollution within urban and agricultural landscapes [*Grathwohl et al*., 2013; *Belmont and Foufoula-Georgiou,* 2017]. In this thesis project I worked with my mentors at UC Irvine (Professors Stanley Grant, Megan Rippy, and PhD graduate student Ms. Morvarid Azizian) to develop, calibrate, and validate a coupled physical and biokinetic model for denitrification in the hyporheic zone of streams [*Grant et al*., 2014; *Azizian et al*. 2015, 2017]. The model is called the Pumping and Streamline Segregation (PASS) model, and accounts for the physical transport of oxygen and dissolved inorganic nitrogen species (DIN, including nitrate and ammonium) between the stream and hyporheic zone (so-called "hyporheic exchange"), as well as biogeochemical transformations that occur as stream water moves through the hyporheic zone. In this thesis the PASS model is calibrated and validated using a unique dataset in which the fundamental processes responsible for nitrogen transformation in the hyporheic zone were systematically evaluated at 72 sites across the U.S. In future work the calibrated and validated PASS model will be used to identify appropriate relationships for the scale-up of denitrification from the bedform to the basin.

2. Methods

2.1 Pumping and Streamline Segregation (PASS) Model

The PASS model is premised on three fundamental assumptions: (1) movement of water through the hyporheic zone is driven by dynamic and/or static pressure variations over periodic fluvial bedforms, such as ripples or dunes; (2) solutes are transported through the hyporheic zone by advection alone (i.e., solute mixing within the hyporheic zone by diffusion and dispersion is neglected, see detailed discussion in *Grant et al*. [2014]); and (3) movement of water and solutes through the hyporheic zone is steady-state. Given these assumptions, mass balance over a single periodic bedform yields the following formula for the nitrate uptake velocity (v_f, units m s^{-1}), defined as the ratio of the flux of nitrate out of the streambed ($U_{NO_3^-}$, units mol m^{-2} s^{-1}) divided by the nitrate concentration in the stream ($C_{S\text{-}NO_3^-}$, units mol m^{-3}):

$$v_f \equiv U_{NO_3^-} / C_{S\text{-}NO_3^-} = -q_H \left[1 - \bar{F}_N\right]$$
$$\bar{F}_N = \int_0^\infty F_N(\tau) E(\tau) d\tau \quad (1)$$

Symbols appearing here include the hyporheic exchange flux (i.e., Darcy flux of water undergoing hyporheic exchange, q_H, units m s^{-1}); the fraction of nitrate remaining after a water parcel passes through the hyporheic zone, referred to here as the fractional nitrate conversion ($F_N(\tau) = C_{NO_3^-}(\tau) / C_{S\text{-}NO_3^-}$, unitless) [*Zarnetske et al*., 2012]; the nitrate concentration of a water parcel in the hyporheic zone after a residence time τ (units s)

($C_{\text{S-NO}_3^-}(\tau)$, units mol m^{-3}); and a flux-weighted residence time distribution ($E(\tau)$ units s^{-1}), defined as the fraction of water circulating through the hyporheic zone that has a residence time within $d\tau$ of τ.

The quantity $\overline{F}_{\text{N}}$ appearing in equation (1) represents the flux-weighted fractional conversion of nitrate, and can take on any positive real value ($0 < \overline{F}_{\text{N}} < \infty$). When the flux-weighted fractional conversion is less than unity ($0 < \overline{F}_{\text{N}} < 1$) the hyporheic zone is a net sink of nitrate and the nitrate uptake velocity is negative in sign ($v_{\text{f}} < 0$). Conversely, if the flux-weighted fractional conversion is greater than unity ($\overline{F}_{\text{N}} > 1$), the hyporheic zone is a net source of nitrate (e.g., by nitrification), and the nitrate uptake velocity is positive in sign ($v_{\text{f}} > 0$). In the limit where $\overline{F}_{\text{N}} = 0$, the rate of nitrate uptake is controlled by the Darcy flux of water across the sediment-water interface; i.e., under these conditions nitrate uptake is mass transfer limited, $v_{\text{f,MTL}} = -q_{\text{H}}$.

Depending on the process of interest, different forms of the nitrate uptake velocity can be defined and calculated from the PASS model. The uptake velocity that appears in equation (1) takes into account both nitrate generation in the hyporheic zone (e.g., by nitrification) and nitrate removal in the hyporheic zone (e.g., by denitrification). Consequently, the sign of v_{f} will determine whether the hyporheic zone is a net sink $(v_{\text{f}} < 0)$ or source $(v_{\text{f}} > 0)$ of nitrate, as indicated above. Alternatively, uptake velocities can be defined as only removal of streamborne nitrate by direct denitrification ($v_{\text{f,Dw}}$) or removal of streamborne ammonium by coupled nitrification-denitrification ($v_{\text{f,Dn}}$)

[*Nielsen*, 1992]. Because these latter two uptake velocities quantify the removal of nitrogen carried by the stream, they are negative in sign and calculated from the model-predicted flux of N_2 out of the streambed (U_{N_2}, units mol m^{-2} s^{-1}) produced by direct denitrification of streamborne nitrate ($v_{f,Dw} = -U_{N_{2,Dw}} / C_{S\text{-}NO_3^-}$) or coupled nitrification-denitrification of streamborne ammonium ($v_{f,Dn} = -U_{N_{2,Dn}} / C_{S\text{-}NO_3^-}$). Finally, the total nitrate uptake velocity represents the removal of streamborne nitrate by denitrification and by plant and microbial assimilation ($v_{f,tot}$, see *Mulholland et al*. [2008]). In this thesis I will focus on modeling the uptake velocity associated with direct denitrification of stream nitrate (i.e., $v_{f,Dw}$) because of its relevance to the ecosystem services (transformation of streamborne nitrate to di-nitrogen gas) and disservices (transformation of streamborne nitrate to nitrous oxide gas) described earlier.

2.2 LINX II Dataset

I calibrated and validated the PASS model using previously published field data collected as part of the second lotic intersite nitrogen experiment (LINX II) [*Mulholland et al*., 2008,2009; *Beaulieu et al*., 2011]. The LINX II study included ^{15}N-labeled nitrate seeding experiments in 72 streams across eight regions of the U.S., collectively representing eight different biomes (temperate rain forest, chaparral, northern mixed forest, deciduous forest, montane coniferous forest, temperate grassland, shrub desert and tropical forest) and three different land-use types (undisturbed or reference sites, urban-impacted sites, and agriculture-impacted sites) [*Mulholland et al*., 2008]. Here I focus on a subset of the LINX II sites where hyporheic exchange is likely to have occurred across fluvial dunes. This focus is warranted because, when hyporheic exchange occurs across dunes, the quantities q_{H} and $E(\tau)$ can be estimated from field measurements of stream velocity and stream width using a simple analytical model (see next section). The dune sites were identified based on the classification scheme proposed by *Marzadri et al*. [2014]; namely, streambed slope $s_0 < 0.009$ and median grain size diameter of the streambed $d_{50} < 4$ mm. Nineteen of the 72 LINX II sites met these two criteria, including four reference sites, seven urban-impacted sites, and eight agriculture-impacted sites.

2.3 Advective Pumping Model for Hyporheic Exchange

In this study I assume hyporheic exchange occurs across fluvial dunes of height H (units m), wavelength λ (units m), and hydraulic conductivity K_h (units m s^{-1}) in a stream of depth d_s (units m) and flow velocity U (units m s^{-1}), as shown in **Figure 1**. Under such conditions, *Boano et al*. [2008, 2009] derived the following advective pumping model for the hyporheic exchange flux, where q_V (units m s^{-1}) is the vertical Darcy flux of groundwater into the stream (gaining conditions, $q_V > 0$) or from the stream into the groundwater (losing conditions, $q_V < 0$):

$$\begin{aligned} q_H &= q_{H,0}\sqrt{1-(q_V/\pi q_{H,0})^2} + \left(|q_V|/\pi\right)\sin^{-1}\left(|q_V|/\pi q_{H,0}\right) - \left(|q_V|/2\right) \\ q_{H,0} &= 2aK_h h_0/\lambda \\ h_0 &= \frac{U^2}{2g}\left(\frac{H}{0.34 d_s}\right)^m \end{aligned} \qquad (2)$$

This physical model assumes that hyporheic exchange is driven by dynamic pressure variations over the surface of a fluvial dune in a turbulent stream, with high-pressure regions at dune troughs (downwelling zones) and low-pressure regions at dune crests (upwelling zones); it is an evolution of similar expressions derived in the absence of ambient groundwater flow [*Vaux*, 1968; *Elliott and Brooks,* 1997a, 1997b]. Additional variables appearing in equation (2) include the gravitational constant ($g = 9.81$ m s^{-2}), two empirical parameters a and m (both unitless), the pressure head perturbation associated with turbulent flow over a dune (h_0, units m), and the hyporheic exchange flux when the stream is neither gaining nor losing ($q_V = 0$) ($q_{H,0}$, units m s^{-1}).

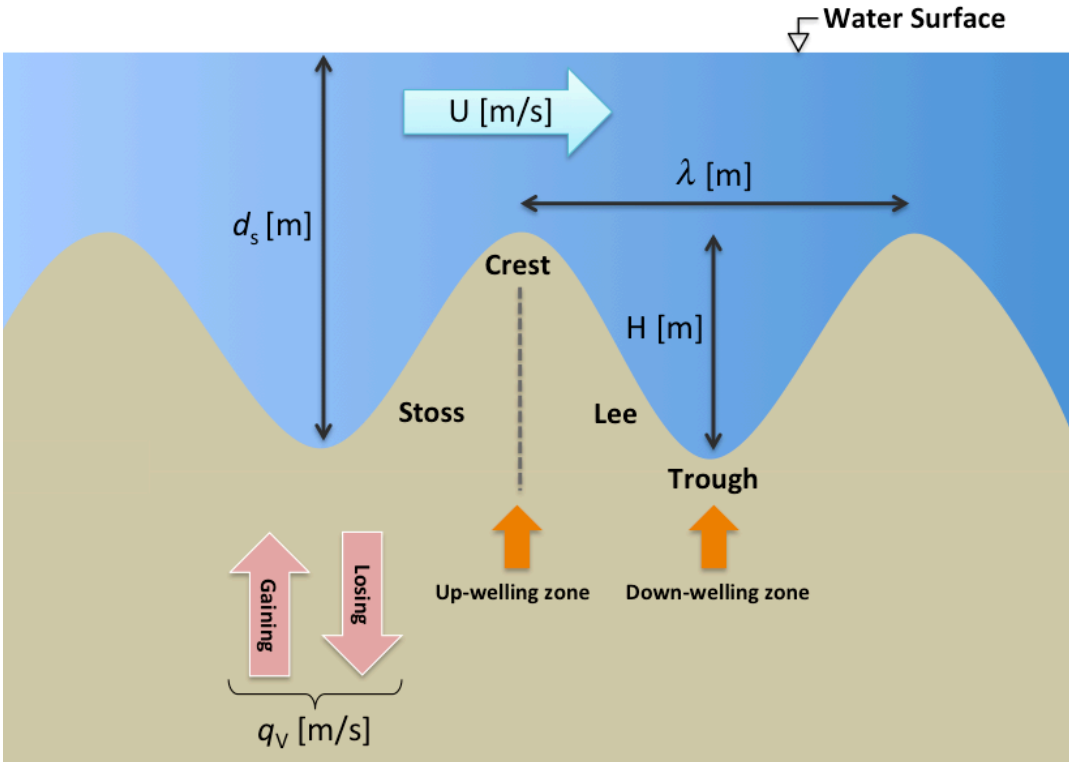

Figure 1: The Advective Pumping Model for Hyporheic Exchange considers the vertical Darcy flux of groundwater (gaining/losing conditions). Low-pressure regions (up-welling zones) are located at the dune crests, whereas high -pressure regions (down-welling zones) are located at dune troughs.

2.4 Biokinetic Model for N-Cycling in the Hyporheic Zone

As oxygen and DIN move through the hyporheic zone they are subject to a variety of microbially mediated redox reactions. In my biokinetic model I capture three of the most important such reactions, including aerobic respiration (AR), denitrification (DN), and nitrification (NI) (*Kessler et al*., [2013]; *Cook et al*., [2006]; *Azizian et al*., [2014; 2017]):

$$\text{Aerobic respiration (AR): } CH_2O + O_2 \rightarrow CO_2 + H_2O \tag{3a}$$

$$R_{AR} = R_{min}\left(\frac{C_{O_2}}{C_{O_2} + K_{O_2}^{sat}}\right) \tag{3b}$$

$$\text{Denitrification (DN): } CH_2O + 0.8NO_3^- + 0.8H^+ \rightarrow CO_2 + 0.4N_2 + 1.4H_2O \tag{3c}$$

$$R_{DN} = \kappa R_{min}\left(\frac{C_{NO_3^-}}{C_{NO_3^-} + K_{NO_3^-}^{sat}}\right)\left(\frac{K_{O_2}^{inh}}{C_{O_2} + K_{O_2}^{inh}}\right) \tag{3d}$$

$$\text{Nitrification (NI): } NH_4^+ + 2O_2 \rightarrow NO_3^- + 2H^+ + H_2O \tag{3e}$$

$$R_{NI} = k_{NI} C_{NH_4^+} C_{O_2} \tag{3f}$$

The rate expressions corresponding to each redox reaction are also indicated. The rate of AR (R_{AR} , units mol m^{-3} s^{-1}, equation (3b)) is proportional to the organic carbon mineralization rate (R_{min} , units mol m^{-3} s^{-1}) and exhibits a Monod (saturation) dependence on interstitial oxygen concentration (C_{O_2} with half saturation constant $K_{O_2}^{sat}$, both units mol m^{-3}). The rate of DN (R_{DN} , units mol m^{-3} s^{-1}, equation (3d)) is proportional to R_{min}

(proportionality constant κ, unitless), exhibits a Monod dependence on interstitial nitrate concentration ($C_{NO_3^-}$ with half saturation constant $K_{NO_3^-}^{sat}$, both units mol m^{-3}), and is non-competitively inhibited by oxygen (inhibition constant of $K_{O_2}^{inh}$, units mol m^{-3}). Finally, the rate of NI (R_{NI}, units mol m^{-3} s^{-1}, equation (3f)) is second-order in both ammonium ($C_{NH_4^+}$) and oxygen concentrations (rate constant k_{NI}, units m^3 mol^{-1} s^{-1}).

Because both AR and DN are proportional to the organic carbon mineralization rate, the latter plays a critical role in determining how quickly nitrate is removed in the hyporheic zone. Various expressions for R_{min} have been proposed in the literature, for example to account for the downwelling of streamborne dissolved organic carbon (DOC) and dissolution of particulate organic carbon (POC) trapped within the streambed (i.e., in situ generation of DOC from POC and its subsequent mineralization) (e.g., see *Zarnetske et al*. [2012] and *Sawyer,* [2015]). Alternatively, *Cook et al.,* [2006] proposed a parsimonious empirical relationship, in which the organic carbon mineralization rate is assumed to decline monotonically with depth into the streambed: $R_{min}(z) = R_{min,0} e^{-(z/z_0)^2}$. Variables in Cook et al.'s model represent the characteristic depth in the sediment over which organic carbon mineralization takes place (z_0, units m), a site-specific mineralization rate at the sediment-water interface ($R_{min,0}$, units mol m^{-3} s^{-1}), and elevation above the streambed (z, units m). I adapted Cook et al.'s empirical model by replacing depth z with residence time in the hyporheic zone τ, and defining a characteristic time for organic carbon mineralization: $\tau_0 = \theta z_0 / q_H$, where θ is streambed porosity, the mineralization depth is $z_0 = 0.1$ m, and q_H is a site-specific hyporheic

exchange flux estimated from the advective pumping model described earlier (see equation (2)).

Under steady-state conditions and neglecting mixing by diffusion and mechanical dispersion (see PASS model assumptions), mass balance over a single water parcel yields a set of coupled non-linear ordinary differential equations for the change in interstitial oxygen, nitrate, and ammonium concentrations with travel time through the hyporheic zone:

$$\frac{dC_{O_2}}{d\tau} = \underbrace{-R_{\min,0}e^{-(\tau/\tau_0)^2}\left(\frac{C_{O_2}}{C_{O_2}+K_{O_2}^{sat}}\right)}_{AR} \underbrace{-2k_{NI}C_{O_2}C_{NH_4^+}}_{NI} \quad (4a)$$

$$\frac{dC_{NO_3^-}}{d\tau} = \underbrace{k_{NI}C_{O_2}C_{NH_4^+}}_{NI} \underbrace{-\kappa R_{\min,0}e^{-(\tau/\tau_0)^2}\left(\frac{K_{O_2}^{inh}}{C_{O_2}+K_{O_2}^{inh}}\right)\left(\frac{C_{NO_3^-}}{C_{NO_3^-}+K_{NO_3^-}^{sat}}\right)}_{DN} \quad (4b)$$

$$\frac{dC_{NH_4^+}}{d\tau} = \underbrace{-k_{NI}C_{O_2}C_{NH_4^+}}_{NI} \quad (4c)$$

$$C_{O_2}(0) = C_{S\text{-}O_2},\ C_{NO_3^-}(0) = C_{S\text{-}NO_3^-},\ C_{NH_4^+}(0) = C_{S\text{-}NH_4^+} \quad (4d)$$

For the set of initial conditions adopted here (equation (4d)), I have assumed that the interstitial concentrations of molecular oxygen, nitrate, and ammonium are equal to their respective ambient stream concentrations ($C_{S\text{-}O_2}$, $C_{S\text{-}NO_3^-}$, and $C_{S\text{-}NH_4^+}$, respectively) as water enters the hyporheic zone from the stream (at $\tau = 0$). **Figure 2** shows the concentrations versus the residence time.

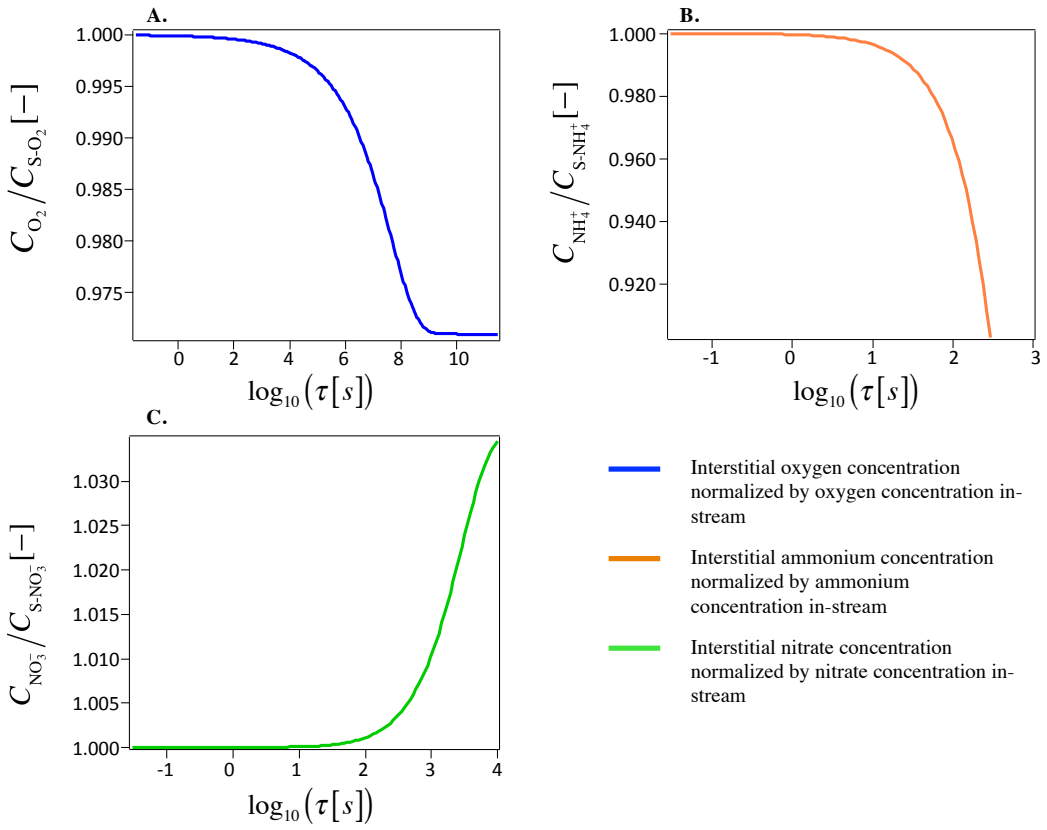

Figure 2: Behavior of the normalized concentrations of (A): oxygen, (B): ammonium and (C): nitrate, with respect to the log-transformed residence time (τ) for one of the LINX II sites (Kimball). For $\tau = 0$, the interstitial concentrations have been considered equal to the ambient stream concentrations ($C_{O_2}/C_{S\text{-}O_2} = 1$; $C_{NH_4^+}/C_{S\text{-}NH_4^+} = 1$; $C_{NO_3^-}/C_{S\text{-}NO_3^-} = 1$).

2.5 Calibrating the Advective Pumping Model

For each of the LINX II sites included in this study, the parameters appearing in equation (2) were either: (a) measured in the field (stream velocity U); (b) taken as a constant based on literature values ($m = 3/8$ [*Elliott and Brooks,* [1997a]; *Fehlman,* [1985]); (c) calculated from field measurements as outlined by *Marzadri et al*. [2014], including stream depth ($d_s = Q/(UW)$ where Q (units $m^3\ s^{-1}$) and W (units m) are measured stream discharge and width, respectively), dune height $H = 0.165 \times d_s$, dune length $\lambda = 6 \times d_s$ [Yalin, 1964], and hydraulic conductivity of the streambed $K_h = 16.88 + 10.6 \times d_{50}$, where d_{50} is the measured median grain size of the streambed [*Salarashayeri and Siosemarde*, 2012]; or (d) estimated from the mass transfer limited uptake of ^{15}N-labeled nitrate measured as part of the LINX II studies (the empirical constant a). Relative to the latter, for sites where nitrate uptake is mass transfer limited and there is negligible groundwater discharge or recharge (i.e., $q_V = 0$), by definition $v_{f,MTL} = -q_{H,0}$ and the parameter a can be obtained by rearranging equation (2):

$$a = -\frac{v_{f,MTL} g \lambda}{K_h U^2} \left(\frac{H}{0.34 d_s} \right)^{-3/8} \qquad (5)$$

Because I do not know *a priori* which LINX II sites are mass transfer limited, I calculated from equation (5) values of a for all seventeen sites included in this study. Then I selected the five largest a values, on the premise that mass transfer limited conditions are most likely to apply when a is maximal. At the end, the median of these values was then selected for further analysis.

Residence time distributions were calculated using the analytical solution derived by *Azizian et al*. [2017], which adopts as a starting point the same hyporheic exchange velocity field utilized in Boano et al.'s solution for the hyporheic exchange flux (equation (2)) (a Mathematica code for implementing this solution for $E(\tau)$ can be found in the Supplemental Information of *Azizian et al*. [2017]). In addition to the hydraulic parameters already discussed, the solution for $E(\tau)$ requires specification of the horizontal (q_{U}) groundwater flux, which I calculated for each LINX II site from the measured stream slope (s_0) and my previously described estimates of hydraulic conductivity ($q_{\mathrm{U}} = K_{\mathrm{h}} \times s_0$).

2.6 Overview of Biokinetic Model Calibration

Altogether, the biokinetic model here requires the specification of six parameters ($K_{O_2}^{sat}$, $K_{NO_3^-}^{sat}$, $K_{O_2}^{inh}$, $R_{min,0}$, k_{NI}, κ). Of these parameters, the last three are probably the most critical, because they are directly proportional to the rates of AR ($R_{min,0}$), DN ($R_{min,0}$, κ), and NI (k_{NI}) (see equations (4a) through (4c)). Accordingly, literature values were adopted for the three saturation parameters ($K_{O_2}^{sat} = 6 \times 10^{-3}$, $K_{NO_3^-}^{sat} = 0.081$, $K_{O_2}^{inh} = 3 \times 10^{-3}$ mol m^{-3} [*Sawyer*, 2015]) while $R_{min,0}$, k_{NI}, and κ were evaluated sequentially from LINX II field measurements in two steps.

In the first step I utilized LINX II measurements of the oxygen uptake velocity (v_{f,O_2}^{field}) to estimate values for $R_{min,0}$ and k_{NI} at the 19 sites where dunes were thought to dominate hyporheic exchange (see earlier). These nineteen sites were divided into three groups based on their ambient stream ammonium concentration (low, high, and reserved). The first two groups were used for model calibration. Sites from the first group were used to estimate $R_{min,0}$ under the assumption that nitrification has little influence on oxygen consumption in the hyporheic zone when stream ammonium concentrations are low. Sites from the second group were used to estimate k_{NI} under the assumption that nitrification will influence oxygen consumption in the hyporheic zone when stream ammonium concentrations are high. The third group was reserved to validate PASS model predictions of oxygen uptake velocity.

In the second step, the parameter κ was estimated from the previously determined values for $R_{\min,0}$ and k_{NI} (obtained from the first step) combined with LINX II measurements of the direct denitrification of stream nitrate ($v_{\mathrm{fden}}^{\mathrm{field}}$, obtained from ^{15}N-labeled nitrate seeding studies, see *Mulholland et al*. [2008]). Of the 19 LINX II sites included in this study, 11 had $v_{\mathrm{fden}}^{\mathrm{field}}$ measurements, and from these six were randomly selected for calibration of the parameter κ. The remaining five sites were reserved to validate PASS model predictions of the direct denitrification of stream nitrate.

2.7 Calibration of $R_{min,0}$ and k_{NI} from Measured Oxygen Uptake Velocity

To estimate values for $R_{min,0}$ and k_{NI} I focused on LINX II measurements of stream ecosystem respiration (ER), which is the flux of oxygen into the streambed resulting from nighttime heterotrophic and autotrophic respiration [*Bernot et al.,* 2010]. By definition, a oxygen uptake velocity for each LINX II site (v_{f,O_2}, units m s^{-1}) can be calculated from the ratio of the measured ER and stream oxygen concentrations: $v_{f,O_2}^{field} = -ER/C_{S\text{-}O_2}$. Corresponding PASS model predictions of the oxygen uptake velocity were calculated as follows:

$$v_{f,O_2}^{PASS} = -q_H\left[1 - \int_0^{\infty} F_{O_2}(\tau)E(\tau)d\tau\right] \quad (6a)$$

$$F_{O_2}(\tau) = C_{O_2}(\tau)/C_{S\text{-}O_2} \quad (6b)$$

$$\frac{dC_{O_2}}{d\tau} = \underbrace{-R_{min,0}\exp\left[-\left(\frac{\tau q_H}{(0.1\text{m})\theta}\right)^2\right]\left(\frac{C_{O_2}}{C_{O_2}+K_{O_2}^{sat}}\right)}_{AR} \underbrace{-2k_{NI}C_{O_2}C_{NH_4^+}}_{NI} \quad (6c)$$

$$\frac{dC_{NH_4^+}}{d\tau} = \underbrace{-k_{NI}C_{O_2}C_{NH_4^+}}_{NI} \quad (6d)$$

$$C_{O_2}(0) = C_{S\text{-}O_2},\ C_{NH_4^+}(0) = C_{S\text{-}NH_4^+} \quad (6e)$$

As currently written, $R_{min,0}$ and k_{NI} are the only unknown parameters in equation (4a)-(4d); all other parameters can be calculated for each LINX II site as outlined earlier. To estimate these two parameters I divided the LINX II sites into three categories: (a) seven sites with the lowest ambient stream ammonium concentration ($C_{S\text{-}NH_4^+} < 1.50\times10^{-3}$ mol m^{-3}); (b) seven sites with the highest ambient stream ammonium concentration

($C_{\text{S-NH}_4^+} > 5.29\times10^{-3}$ mol m^{-3}); and (c) all remaining sites ($1.50\times10^{-3} < C_{\text{S-NH}_4^+} < 5.29\times10^{-3}$ mol m^{-3}). Because group (a) has relatively low ambient ammonium concentration, the contribution of nitrification to oxygen consumption is likely to be minimal, and thus a simplified form of equation (6c) is adopted:

$$\frac{dC_{O_2}}{d\tau} \approx \underbrace{-R_{\min,0}\exp\left[-\left(\frac{\tau q_H}{(0.1\text{m})\theta}\right)^2\right]\left(\frac{C_{O_2}}{C_{O_2}+K_{O_2}^{sat}}\right)}_{AR} \tag{7}$$

In this case, the only unknown is $R_{\min,0}$, which can be found by solving for the value that yields a match between the predicted and measured uptake velocity at each site in group (a): $v_{f,O_2}^{PASS}\big|_{R_{\min,0}} = v_{f,O_2}^{field}$. The seven realizations of $R_{\min,0}$ thus obtained were then regressed against ER and gross primary production (GPP)—both fundamental measures of stream metabolism [*Bernot et al.*, 2010]. Either the median value of $R_{\min,0}$ or its empirical relationship with ER and/or GPP (if statistically significant) was adopted for all subsequent calculations.

Once $R_{\min,0}$ was calibrated, I used the PASS model to find estimates for the nitrification rate constant k_{NI} based on oxygen uptake measurements at group (b) sites (see above). For each of the sites in group (b), I found the k_{NI} value that yields a match between the predicted and measured oxygen uptake velocity: $v_{f,O_2}^{PASS}\big|_{k_{NI}} = v_{f,O_2}^{field}$. The realizations of k_{NI} were regressed against ER and GPP, and depending on the outcome either the median value or an empirical relationship with ER and/or GPP (if statistically significant) was adopted for all subsequent calculations.

2.8 Calibration of κ from Direct Denitrification of Streamborne Nitrate

Out of the 19 LINX II sites included in this study, measurements of the uptake velocity for direct denitrification of streamborne nitrate ($v_{f,den}^{field}$) were available for 11 sites, including two reference sites, three agriculture-impacted sites, and six urban-impacted sites (for a variety of reasons, LINX II researchers could not estimate at all sites, see *Mulholland et al*. [2008]). From these 11 sites, six sites were randomly selected to calibrate κ as follows. The 11 sites were arrayed from the lowest to the highest in-stream ammonium concentration and assigned a number between 0 (for the first site) and 1 (for the last site) in increments of 0.1. A random number was then selected (Matlab, Mathworks, MA) and the LINX II site with an assigned value closest to the random number was selected for the calibration group. This process was continued for the remaining sites until six calibration sites were selected. For each of these calibration sites I solved for the corresponding value of κ that yielded a match between PASS model-predictions and field measurements of direct denitrification of stream nitrate: $v_{f,Dw}^{PASS}\big|_{\kappa} = v_{f,den}^{field}$. Model predictions for $v_{f,Dw}^{PASS}$ were obtained by calculating the flux of dinitrogen gas associated with the direct denitrification of streamborne nitrate ($U_{N_2,Dw}$): $v_{f,Dw}^{PASS} = -2U_{N_2,Dw}/C_{S\text{-}NO_3^-}$ (see the Supplemental Information of *Azizian et al*. [2015] for details).

2.9 Validation of PASS Model Predictions

The performance of the PASS model was evaluated as follows. The calibrated model was used to generate predictions for v_{f,O_2}^{PASS} and $v_{f,Dw}^{PASS}$ at all sites where these two uptake velocities were measured (including sites used for model calibration and sites held in reserve for model validation, see above). The model-predicted and measured uptake velocities were then cross-plotted and model performance evaluated using the Nash-Sutcliff efficiency; this index ranges from $-\infty$ to 1, where 1 is a perfect model fit, 0 is no better than the mean, and < 0 is worse than the mean [*Krause et al*., 2005].

2.10 Statistical Analyses

To determine if the three calibrated parameters ($R_{\min,0}$, k_{NI}, and κ, see above) are correlated with ER and/or GPP a multiple linear regression (MLR) was conducted in R software [*R Core Team*, 2013]. Prior to performing the MLR, the variance inflation factor (VIF) was calculated for GPP and ER to evaluate multicolinearity. No significant multicolinearity was detected (VIF < 5) [*Zuur et al*., 2010], indicating that both variables were suitable for co-evaluation in the MLR analyses. Models were ranked using the Bayesian Information Criterion (BIC) [*Schwarz,* 1978] and then further evaluated relative to predictive ability using leave-one-out cross validation with Root Mean Squared Error (RMSE) as the validation metric [*Hawkins et al*., 2003]. When BIC and RMSE did not agree, the final best-fit model was the model with the lowest average RMSE (weighted average across all leave-one-out estimates). The coefficient of determination (R^2) was calculated for each the best-fit model (for $R_{\min,0}$, k_{NI}, and κ, respectively) as an indicator of overall model fit. The relative importance of each predictor variable (i.e., the proportionate contribution made to R^2) was estimated using the averaging over ordering method proposed by Lindeman, Merenda and Gold [*Gromping*, 2006]. In instances where calibrated parameters were not correlated with GPP and/or ER, a median value was utilized and a distribution of means was prepared using bootstrap techniques (Matlab, Mathworks, MA).

3. Results

3.1 Calibrating the Hyporheic Exchange Flux

The constant of proportionality a for the advective pumping model was estimated from LINX II measurements of the total uptake velocity ($v_{f,tot}$), where the latter represents the rate at which ^{15}N-labeled nitrate is removed from the stream by both denitrification and microbial and plant assimilation [*Mulholland et al.,* 2008]. The top five values (corresponding to sites that are most likely to be mass transfer limited, see methods) yield a median value of $a = 0.68$ with lower and upper 95% CIs of 0.35 and 0.99, respectively (**Figure 3A**). Similar median values for a are obtained if, instead of retaining the top five values, the top four or six values are retained (median values of $a = 0.80$ or 0.59, respectively). Note previously published laboratory estimates for a fall below the limit of the CIs I am reporting here [e.g., *Fehlman et al.*, 1985 ($a = 0.28$); and *Fox et al.,* 2014 ($a = 0.16$)].

3.2 Calibrating the Organic Carbon Mineralization Rate

The organic carbon mineralization rate at the sediment-water interface ($R_{min,0}$) was estimated at 7 LINX II sites with low ammonium concentrations (on the premise that nitrification could be neglected at these sites, see methods). MLR of the resulting $R_{min,0}$ values indicate that this parameter is significantly inversely correlated with ER ($R^2 = 0.94$, $p = 0.0003$, $d.o.f. = 5$) (**Figure 3B**) and well-described by the following power-law relationship (solid line in the figure): $R_{min,0} = 10^{3.04 \pm 0.79} \mathrm{ER}^{1.26 \pm 0.14}$.

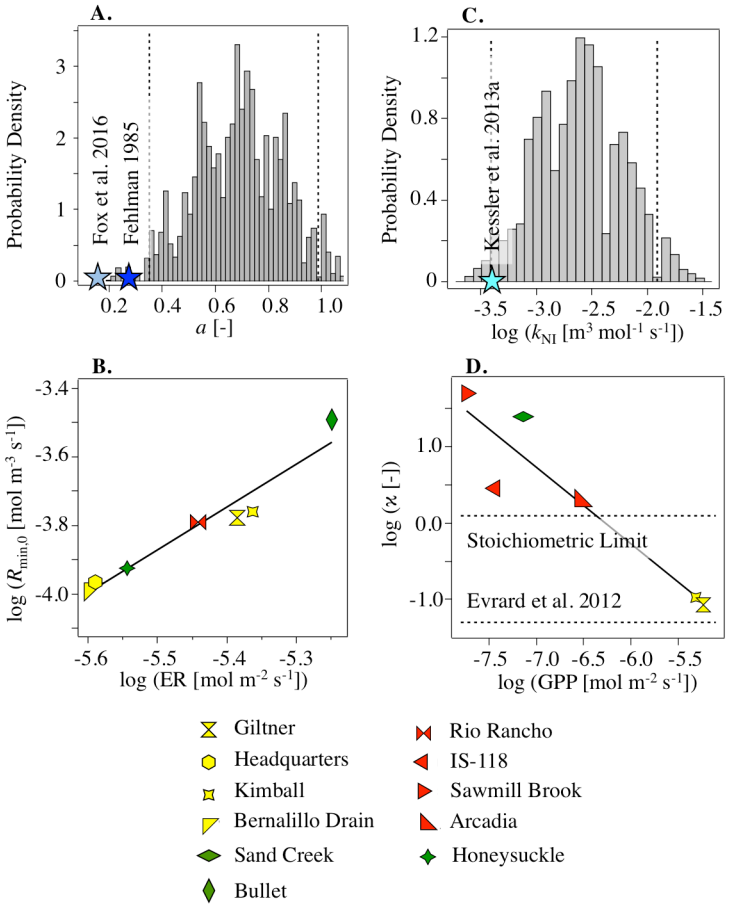

Figure 3: Calibrating the PASS model parameters with the LINXII data **(A)** distribution and 95% confidence intervals (dashed vertical lines) for the mean of the top five selected a values computed by bootstrap technique. Light blue and dark blue stars represent the magnitude of a reported in Fox et al. (2014) and Fehlman (1989), respectively; (B) correlation between the organic carbon mineralization rate at the sediment-water interface ($R_{\min,0}$) for the selected sites and the ecosystem respiration (ER); (C) distribution and 95% confidence intervals (dashed vertical lines) for the mean of selected sites k_{NI} values computed by bootstrap technique. Turquoise star represents the magnitude of k_{NI} reported in Kessler et al. (2013a); (D) correlation between κ for the selected sites and the gross primary production (GPP). Dashed lines present the stoichiometric limit ($\kappa = 1.25$) and reported value in *Evrard et al.* [2012] ($\kappa = 0.05$). In panels (B) and (D), different sites are color-coded with respect to their land use, namely reference streams (green), urban-impacted streams (red), and agricultural-impacted streams (yellow).

3.3 Calibrating the Nitrification Rate Constant

The 7 LINX II sites with the highest ammonium concentrations were selected for estimating the second-order nitrification rate constant (k_{NI}) (see methods). However, k_{NI} values could not be found at two of the sites (DORR and IS_104) because my model-predicted uptake oxygen velocities did not converge to the corresponding measured values; k_{NI} values were successfully obtained for the other five sites. MLR analysis reveals that $\log k_{NI}$ is not significantly correlated with either logER nor logGPP ($p > 0.18$). Therefore the median value of $k_{NI} = 10^{-2.67}$ m^3 mol^{-1} s^{-1} was selected for subsequent calculations (lower and upper 95% CI of $10^{-3.4}$ and $10^{-1.9}$, **Figure 3C**). Note the lower CI is equal to previously published laboratory estimates for k_{NI} [e.g., *Kessler et al.*, 2013a].

3.4 Calibrating the Rate of Nitrate Reduction

I estimated κ values from field measurements of the direct denitrification of stream nitrate (v_{fden}) at 6 of the LINX II sites where hyporheic exchange occurred predominantly across fluvial dunes (the remaining 5 sites were reserved for model validation). The smallest of these realizations ($\kappa = 0.08$) is close to the non-stoichiometric value ($\kappa = 0.05$) reported by *Evrard et al.* [2012], the median ($\kappa = 2.75$) is close to the stoichiometric value ($\kappa = 1.25$), while the maximum ($\kappa = 51$) is well above previously published estimates. Interestingly, the MLR reveals that $\log\kappa$ is significantly inversely correlated with $\log\mathrm{GPP}$ (**Figure 3D**, $R^2 = 0.88$, $p = 0.006$, $d.o.f. = 4$). The observed inverse relationship between κ and GPP can be represented by the following power-law correlation (solid line in **Figure 3D**): $\log\kappa = a - b\log\mathrm{GPP}$ where $a = -6.3 \pm 1.3$ and $b = 1.00 \pm 0.2$ (bounds are standard error).

4. Discussion

4.1 Hyporheic Exchange Flux Calibration

The advective pumping model [*Boano et al.*, 2007, 2008] was used to estimate the hyporheic exchange flux q_H at 19 LINX II sites where fluvial dunes dominate hyporheic exchange. While most of the parameter values needed to estimate q_H are either measured or calculated from field measurements (see methods), there is uncertainty regarding the constant of proportionality between the dynamic pressure head perturbation associated with turbulent flow over a dune and the corresponding hyporheic exchange flux (i.e., the parameter a, see equation (2)). Laboratory flume experiments yield different values for this parameter ($a = 0.28$ and 0.14 according to *Fehlman* [1985] and *Fox et al.* [2016], respectively), and it is not clear that lab-scale experiments can be extrapolated to the field.

The median value for this parameter ($a = 0.68$) is significantly larger, but within a factor of five, of the earlier laboratory estimates. There are several possible explanations for this observation, including: (1) the laboratory values were obtained using a single bedform scale (e.g., ripples of a defined size), whereas in the field hyporheic exchange flux may be additive over multiple bedform scales (e.g., ripples and dunes) [*McCluskey et al.*, 2016]; (2) at the LINX II sites hyporheic exchange may have contributions from both dynamic pressure variations (accounted for in the advective pumping model) and static pressure variations (e.g., associated with the ponding of water behind obstacles in a

stream, not accounted for by the advective pumping model) which could drive additional hyporheic exchange; and (3) the measured total uptake velocities used to estimate a may include nitrate removal processes (such as nitrate uptake by benthic algae) that are not necessarily associated with hyporheic exchange.

4.2 Biokinetic Model Calibration

Calibration of the biokinetic model involved estimating values (or correlations) for three key parameters that determine the rates of organic carbon mineralization ($R_{\min,0}$), nitrification (k_{NI}), and denitrification (κ). Perhaps not surprisingly given that $R_{\min,0}$ was calculated from the oxygen uptake velocity (which, in turn, is calculated from the ratio of ER and $C_{\mathrm{S\text{-}O_2}}$), values of $R_{\min,0}$ are significantly and positively correlated with ER over a several log-cycle change in both variables.

This result is significant for several reasons. First, ER can be easily estimated for any stream from diurnal (e.g., at a frequency of 1 min^{-1}) measurements of stream oxygen concentration (see *Bernot et al.,* [2010]). Therefore the simple correlation between ER and $R_{\min,0}$ provides a tool to generalize my results beyond the limited sites analyzed here, to potentially many other streams. Secondly, this result underscores the importance of stream metabolism, of which ER is a component, in the cycling of nitrogen in the hyporheic zone. Indeed, the importance of ER on N-cycling in streams has already been documented for the LINX II sites using statistical regression models and structural equation models (SEMS). However, to our knowledge, my results are the first to show

how key biokinetic parameters depend strongly on stream metabolism as represented by night-time autotrophic and heterotrophic respiration.

Indeed, even stream gross primary production plays a role in the biokinetics of N-cycling, apparently by modulating, during denitrification, the moles of nitrate reduced per moles of carbon oxidized, as represented by the biokinetic model parameter κ. Aerobic respiration should consume one mole of organic carbon for every mole of molecular oxygen reduced, while denitrification should consume $\kappa = 1/0.8 = 1.25$ moles of organic carbon for every mole of nitrate reduced. However, recent laboratory and field observations of respiratory denitrification in coastal marine sediments indicate that κ is 25 times smaller ($\kappa = 0.05$) than the stoichiometric value ($\kappa = 1.25$) [*Evrard et al.*, 2012; *Kessler et al.,* 2013a, 2013b], perhaps reflecting the dominance of benthic algal metabolism in these systems [*Bourke et al.,* 2017]. Remarkably, the observed inverse correlation between κ and GPP is consistent with the idea that benthic algal metabolism may play a role in the non-stoichiometric reduction of nitrate at the LINX II sites. More generally, these results suggests that two of the primary processes responsible for N-cycling in the hyporheic zone of stream—aerobic respiration of organic material and the stoichiometry of denitrification—are largely determined by the metabolic state of the stream, as represented by ER and GPP.

4.3 PASS Model Validation

For the last step of my analysis, the performance of the PASS model was evaluated by comparing model predictions for v_{f,O_2}^{PASS} and $v_{f,Dw}^{PASS}$ with the reported values at all LINXII sites where these two uptake velocities were measured (including sites used for model calibration and sites held in reserve for model validation, see above). All the data points are aligned along the one-to-one line on the cross-plot of oxygen uptake velocities (**Figure 4A**) and the Nash-Sutcliff efficiency calculated for this set of results present a very good agreement between the model predicted values and measured values at the sites of LINX II study (NSE = 0.67). At the end, I compared model predictions for the direct denitrification uptake velocity with the reported data in LINXII study. The cross-plot of the model-predicted values versus the reported values presents a satisfactory agreement between the model and the actual values (NSE = 0.20) (**Figure 4B**). Since the nitrate uptake velocity calculations capture more complexities of the nitrogen cycling in the sediment, the results of the predicted values for this set of data may not seem as good as the ones reported for the oxygen uptake velocity. Better predictions on nitrate uptake velocity from PASS model requires more understanding about the complexities of the chemistry and physics of the nitrogen cycling in the hyporheic zone of the real systems, such as the ones that are reported in LINXII data set, and is an on-going development process.

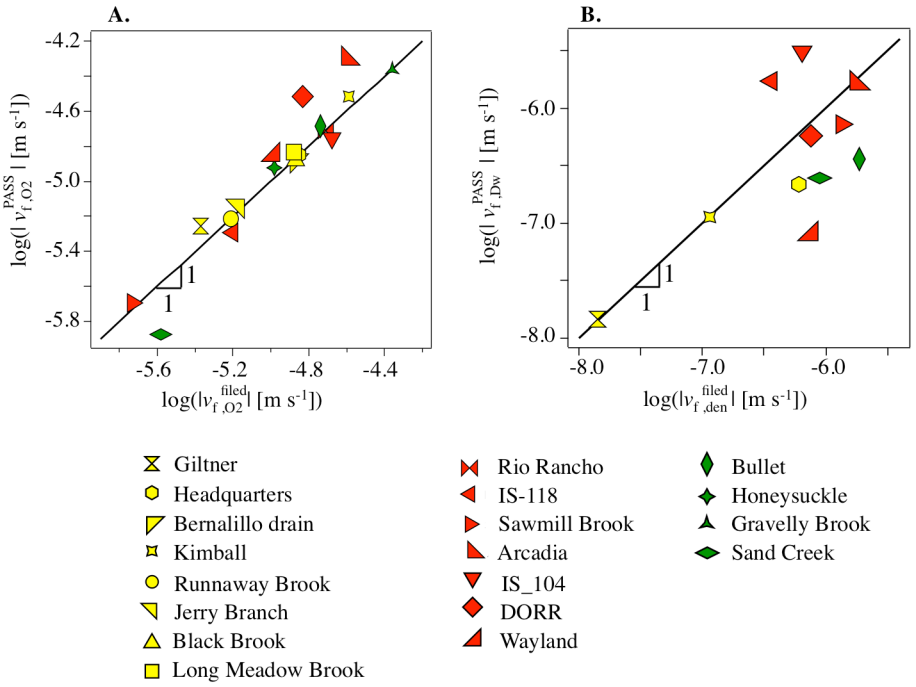

Figure 4: Validation of model (A) Calculated uptake velocity of oxygen from PASS model (v_{f,O_2}^{PASS} , units m s^{-1}) versus uptake velocity of oxygen reported by LINX II study (v_{f,O_2}^{field} , units m s^{-1}); (B) Calculated direct denitrification uptake velocity from PASS model ($v_{f,DW}^{PASS}$, units m s^{-1}) versus direct denitrification uptake velocity reported by LINX II study (v_{fden}^{field} , units m s^{-1}). In both panels, solid line represents the one-to-one line and different sites are color-coded with respect to their land use, namely reference streams (green), urban-impacted streams (red), and agricultural-impacted streams (yellow).

5. Conclusions and Future Directions

In this study I successfully calibrated and validated a process-based coupled physical- and biokinetic model of N-cycling in the hyporheic zone of streams. As a next step my mentors and I plan to employ the validated model to simulate uptake velocities for a wide range of stream chemistry, stream hydrology, and groundwater hydrology. The predictive power of several key time scales (including the median residence time of water in the hyporheic zone, an ER timescale, and a GPP time scale) will be evaluated, with the goal of identifying a universal scaling relationship for several forms of the nitrate uptake velocity. These new results, together with the results presented in this thesis, will be drafted into a journal manuscript and submitted for possible publication.

References

Azizian, M., S.B. Grant, A.J. Kessler, P.L.M. Cook, M.A. Rippy, M. Stewardson (2015), Bedforms as biocatalytic filters: A Pumping and Stream- line Segregation (PASS) model for nitrate removal in permeable sediments, *Environ. Sci. Technol., 49(18),* 10,993–11,002, doi: 10.1021/ acs.est.5b01941.

Azizian, M., F. Boano, P. L. M. Cook, R. L. Detwiler, M. A. Rippy, and S. B. Grant (2017), Ambient groundwater flow diminishes nitrate processing in the hyporheic zone of streams, *Water Resour. Res.,* doi: 10.1002/2016WR020048.

Beaulieu, J. J., J. L. Tank, S. K. Hamilton, W. M. Wollheim, R. O. Hall Jr., P. J. Mulholland, B. J. Peterson, L. R. Ashkenas, L. W. Cooper, C. N. Dahm, W. K. Dodds, N. B. Grimm, S. L. Johnson, W. H. McDowell, G. C. Poole, H. M. Vallet, C. P. Arango, M. J. Bernot, A. J. Burgin, C. L. Crenshaw, A. M. Helton, L. T. Johnson, J. M. O'Brien, J. D. Potter, R. W. Sheibley, D. J. Sobota and S. M. Thomas (2011), Nitrous oxide emission from denitrification in stream and river networks, *Proc. Natl. Acad. Sci. U.S.A.*, *108*(1), 214–219.

Belmont, P. and E. Foufoula-Georgiou (2017), Solving water quality problems in agricultural landscapes: New approaches for these nonlinear, multiprocess, multiscale systems, *Water Resour. Res.*, doi: 10.1002/2017WR020839.

Bernot, M. J., D. J. Sobota, R. O. Hall Jr., P. J. Mulholland, W. K. Dodds, J. R. Webster, J. L. Tank, L. R. Ashkenas, L. W. Cooper, C. N. Dahm, S. V. Gregory, N. B. Grimm, S. K. Hamilton, S. L. Johnson, W. H. McDowell, J. L. Meyer, B. Peterson, G. C. Poole, H. M. Valett, C. Arango, J. J. Beaulieu, A. J. Burgin, C. Creshaw, A. M. Helton, L. Johnson, J. Merriam, B. F. Niederlehner, J. M. O'Brien, J. C. Potter, R. W. Sheibley, S. M. Thomas and K. Wilson (2010), Inter-regional comparison of land-use effects on stream metabolism, *Freshwater Biology*, 55, 1874-1890.

Boano, F., R. Revelli, and L. Ridolfi (2009), Quantifying the impact of groundwater discharge on the surface-subsurface exchange*, Hydrol. Processes,* 23, 2108–2116.

Boano, F., J. W. Harvey, A. Marion, A. I. Packman, R. Revelli, L. Ridolfi, and A. Worman (2014), Hyporheic flow and transport processes: Mechanisms, models, and biogeochemical implications, *Rev. Geophys.,* 25, 603–679, doi:10.1002/2012RG000417.

Bourke, M. F., P. J. Marriott, R. N. Glud, H. Hassler-Sheetal, M. Kamalanathang, J.

Beardall, C. Greening, and P. L. M. Cook (2017), Metabolism in anoxic permeable sediments is dominated by eukaryotic dark fermentation, *Nat. Geosci.*, 10, 30–35.

Bouwman, A. F., G. Van Drecht, and K. W. Van der Hoek (2005), Global and Regional Surface Nitrogen Balances in Intensive Agricultural Pro- duction Systems for the Period 1970-2030, *Pedosphere, 15*, 137–155.

Burgin, A. J., and S. K. Hamilton (2007), Have we overemphasized the role of denitrification in aquatic ecosystems? A review of nitrate removal pathways, *Front. Ecol.Environ.*, 5(2), 89–96.

Cai, W. J., X. P. Hu, W. J. Huang, M. C. Murrell, J. C. Lehrter, S. E. Lohrenz, W. C. Chou, W. D. Zhai, J. T. Hollibaugh, Y. C. Wang, P. S. Zhao, P.S., X. H. Guo, K. Gundersen, M. H. Dai and G.C Gong (2011). Acidification of subsurface coastal waters enhanced by eutrophication, *Nat. Geosci., 4*, 766-770.

Canfield, D. E., A. N. Glazer, and P. G. Falkowski (2010), The evolution and future of earth's nitrogen cycle, *Science, 330*, 192–196.

Carey, R. O., and K. W. Migliaccio (2009), Contribution of wastewater treatment plant effluents to nutrient dynamics in aquatic systems: A review, *Environ. Manage.*, 44, 205-217.

Chan, F., A. B. Boehm, J. A. Barth, E. A. Chornesky, A. G. Dickson, R. A. Feely, B. Hales, T. M. Hill, G. Hofmann, D. Ianson, T. Klinger, J. Largier, J. Newton, T. F. Pedersen, G. N. Somero, M. Sutula, W.W. Wakefield, G. G. Waldbusser, S. B. Weisberg, and E.A. Whiteman (2016), The West Coast Ocean Acidi cation and Hypoxia Science Panel: Major Findings, Recommendations, and Actions, *California Ocean Science Trust*, Oakland, California, USA. April 2016.

Cook, P. L. M., F. Wenzhofer, S. Rysgaard, O. S. Galaktionov, F. J. R. Meysman, B. D. Eyre, J. Cornwell, M. Huettel, and R. N. Glud (2006), Quantification of denitrification inpermeable sediments: Insights from a two-dimensional simulation analysis and experimental data, *Limnol. Oceanogr. Methods*, 4, 294–307.

Elliott, A. H., and N. H. Brooks (1997a), Transfer of nonsorbing solutes to a streambed with bed forms: Theory, *Water Resour. Res.*, 33, 1232136.

Elliott, A. H., and N. H. Brooks (1997b), Transfer of nonsorbing solutes to a streambed with bed forms: Laboratory experiments, *Water Resour. Res.*, 33, 1372151.

Evrard, V., R. N. Glud, and P. L. M. Cook (2012), The kinetics of denitrification in permeable sediments, *Biogeochemistry*, 113, 563–572, doi: 10.1007/s10533-012-9789-x.

Fehlman, H. (1985), Resistance components and velocity distributions of open channel flows over bedforms, MS thesis, Colo. State Univ., Fort Collins.

Galloway, J. N., F. J. Dentener, D. G. Capone, E. W. Boyer, R. W. Howarth, S. P. Seitzinger, G. P. Asner, C. C. Cleveland, P. A. Green, E. A. Holland, D. M. Karl, A. F. Michaels, J. H. Porter, A. R. Townsend and C. J. Vöosmarty (2004), Nitrogen cycles: Past, present, and future, *Biogeochemistry*, 70, 153–226.

Garcia-Ruiz, R., S. N. Pattinson, and B. A.Whitton (1998), Kinetic parameters of denitrification in a river continuum, *Appl. Environ. Microbiol.*, 64, 2533–2538.

Gomez-Velez, J. D., J. W. Harvey, M. B. Cardenas, and B. Kiel (2015), Denitrification in the Mississippi River network controlled by flow through river bedforms, *Nat. Geosci.*, 8, 941–945, doi:10.1038/ngeo2567.

Gooseff, M. N. (2010), Defining hyporheic zones: Advancing our conceptual and operational definitions of where stream water and ground- water meet, *Geogr. Compass*, 4(8), 945–955, doi:10.1111/j.1749-8198.2010.00364.x.

Grant, S. B., K. Stolzenbach, M. Azizian, M. J. Stewardson, F. Boano, and L. Bardini (2014), First-order contaminant removal in the hyporheic zone of streams: Physical insights from a simple analytical model, *Environ. Sci. Technol.*, 48, 11,369–11,378.

Grathwohl, P., H. Rügner, T. Wöhling, K. Osenbrück, M. Schwientek, S. Gayler, U. Wollschläger, B. Selle, M. Pause, J-O. Delfs, M. Grzeschik, U. Weller, M. Ivanov, O. A. Cirpka, U. Maier, B. Kuch, W. Nowak, V. Wulfmeyer, K. Warrach-Sagi, T. Streck, S. Attinger, L. Bilke, P. Dietrich, J. H. Fleckenstein, T. Kalbacher, O. Kolditz, K. Rink, L. Samaniego, H-J. Vogel, U, Werban and G. Teutsch (2013), Catchments as reactors: A comprehensive approach for water fluxes and solute turnover, *Environ. Earth Sci.*, 69, 317–333.

Gromping, U. (2006), Relative Importance for Linear Regression in R: The Package relaimpo. *J.Stat. Softw.*, 17 (1), 1-27.

Hancock, P. J. (2002), Human impacts on the stream-groundwater exchange zone, *Environ. Manage.*, 29, 763–781.

Harms, T. K. and N. B. Grimm (2008), Hot spots and hot moments of carbon and

nitrogen dynamics in a semiarid riparian zone, *Journal of Geophysical Research, 113*, doi:10.1029/2007JG000588.

Harvey, J. W., J. K. Bohlke, M. A. Voytek, D. Scott, and C. R. Tobias (2013), Hyporheic zone denitrification: Controls on effective reaction depth and contribution to whole-stream mass balance, *Water Resour. Res.*, 49, 6298–6316, doi:10.1002/wrcr.20492.

Hawkins, D. M., S. C. Basak, D. Mills (2003), Assessing model fit by cross-validation, *J. Chem. Inf. Comput. Sci.,* 43, 579-586.

Herzog, S. P., C. P. Higgins, and J. E. McCray (2015), Engineered streambeds for induced hyporheic flow: Enhanced removal of nutrients, pathogens, and metals from urban streams, *ASCE J. Environ. Eng.*, 142(1), 04015053.

Hu, B. L., L. D. Shen, X. Y. Xu, and P. Zheng (2011), Anaerobic ammonium oxidation (anammox) in different natural ecosystems, *Biochem. Soc. Trans.*, 39(6), 1811–1816.

Jongbloed, A. W., and N. P. Lenis (1998), Environmental concerns about animal manure, *J. Anim. Sci.*, 76(10), 2641–2648.

Kaushal, S. S., P. M. Groffman, P. M. Mayer, E. Striz, E. J. Doheny, and A. J. Gold (2008), Effects of stream restoration on denitrification in an urbanizing watershed, *Ecol. Appl.* 18, 789–804.

Keeling, R. F., A. Körtzinger, and N. Gruber (2010), Ocean deoxygenation in a warming world, *Annual Review of Marine Science, 2*,199-229.

Kessler, A. J., R. N. Glud, M. B. Cardenas, and P. L. M. Cook (2013a), Transport zonation limits coupled nitrification-denitrification in permeable sediments, *Environ. Sci. Technol.,* 47, 13,404–13,411.

Kessler, A. J., R. N. Glud, M. B. Cardenas, M. Larsen, M. F. Bourke, and P. L. M. Cook (2013b), Quantifying denitrification in rippled permeable sands through combined flume experiments and modeling, *Limnol. Oceanogr.,* 57, 1217–1232.

Kiel, B. A., and M. B. Cardenas (2014), Lateral hyporheic exchange throughout the Mississippi River network, *Nat. Geosci.*, 7(6), 413–417.

Krause, P., Boyle, D.P., Base, F. (2005) "Comparison of different efficiency criteria for hydrological model assessment" *Adv. Geosci.* 5, 89-97.

Kroeze, C., A. Moiser, and L. Bouwman (1999), Closing the global N_2O budget: A retrospective analysis 1500–1994, *Global Biogeochem. Cycles*, *13*(1), 1–8.

Lansdown, K., B. A. McKew, C. Whitby, C. M. Heppell, A. J. Dumbrell, A. Binley, L. Olde, and M. Trimmer (2016), Importance and controls of anaerobic ammonium oxidation influenced by riverbed geology, *Nat. Geosci.*, 9, 357–360, doi:10.1038/ngeo2684.

Lassaletta, L., H. García-Gómez, B. S. Gimeno and J. V. Rovira (2009), Agriculture-induced increase in nitrate concentrations in stream waters of a large Mediterranean catchment over 25 years (1981–2005), *Elsevier*, 47, 6034-6043.

Marzadri A, Tonina D, Bellin A, Tank JL (2014) A hydrologic model demonstrates nitrous oxide emissions depend on streambed morphology. *Geophys Res Lett* 41:5484–5491, doi: 10.1002/2014GL060732.

Marzadri, A., M. M. Dee, D. Tonina, A. Bellin and J. L. Tank (2017), Role of surface and subsurface processes in scaling N_2O emissions along riverine networks, *PNAS*.

McClain, M. E., E. W. Boyer, C. L. Dent, S. E. Gergel, N. B. Grimm, P. M. Groffman, S. C. Hart, J. W. Harvey, C. A. Johnston, E. Mayorga, W. H. McDowell, and Gilles Pinay (2003), Biogeochemical hot spots and hot moments at the interface of terrestrial and aquatic ecosystems, *Ecosystems*, 6, 301-312, doi: 10.1007/s10021-003-0161-9.

McCluskey, A. H., Grant, S. B., and Stewardson, M. J. (2016), Flipping the thin film model: Mass transfer by hyporheic exchange in gaining and losing streams, *Water Resour. Res.*, 52(10), 7806-7818.

Mulholland, P. J., et al. (2008), Stream denitrification across biomes and its response to anthropogenic nitrate loading, *Nature*, 452, 202–205.

Mulholland, P. J., et al. (2009), Nitrate removal in stream ecosystems measured by 15N addition experiments: Denitrification, *Limnol. Oceanogr.,* 54(3), 666–680.

National Academy of Engineering (2017), NAE Grand Challenges for Engineering. [online] Available at: http://www.engineeringchallenges.org/challenges.aspx [Accessed 30 May, 2017].

Nielsen, L. P. (1992) Denitrification in sediment determined from nitrogen isotope pairing, *FEMS Microbiology Letters*, 86(4), 357-362.

Peterson, B., et al. (2001), Control of nitrogen export from watershed by headwater

streams, Nature, *292*, 86–89.

R core team (2013). R: A language and environment for statistical computing. R Foundation for Statistical Computing, Vienna, Austria. ISBN 3-90051-07-0, Available at: http://www.R-project.org/ [Accessed 30 May, 2017]

Ryther, J. H. and W. M Dunstan (1971), Nitrogen, Phosphorus, and Eutrophication in the Coastal Marine Environment, *Science, 171*, 1008-1013, doi: 10.1126/science.171.3975.1008.

Salarashayeri, A. F., and M. Siosemarde (2012), Prediction of soil hydraulic conductivity from particle-size distribution, *World Acad. Sci. Eng. Technol.*, *61*, 454–458.

Sawyer, A. H. (2015), Enhanced removal of groundwater-borne nitrate in heterogeneous aquatic sediments, *Geophys. Res. Lett.,* 42, 403– 410, doi:10.1002/2014GL062234.

Schot, P. P. and J. van der Wal (1992), Human impact on regional groundwater composition through intervention in natural flow patterns and changes in land use, *Elsevier,* 134, 297-313, doi: 10.1016/0022-1694(92)90040-3.

Schwarz, G. (1978), Estimating the dimension of a model, *Ann. Statist., 6*, 461-464

Seitzinger, S., J. A. Harrison, J. K. Bohlke, A.F. Bouwman, R. Lowrance, B. Peterson, C.Tobias, and G. Van Drecht (2006), Denitrification across Landscapes and Waterscapes: A Synthesis, *Ecol. Appl., 16*, 2064–2090.

Smith, V. H., G. D. Tilman, and J. C. Nekola (1999), Eutrophication: Impacts of excess nutrient inputs on freshwater, marine, and terrestrial ecosystems, *Environ. Pollut., 100*, 179–196.

Steffen, W., K. Richardson, J. Rockström, S. E. Cornell, I. Fetzer, E. M. Bennett, R. Biggs, S. R. Carpenter, W. de Vries, C. A. de Wit, C. Folke, D. Gerten, J. Heinke, G. M. Mace, L. M. Persson, V. Ramanathan, B. Reyers and S. Sörlin (2015), Planetary boundaries: Guiding human development on a changing planet, *Sience, 347*, doi: 10.1126/science.1259855.

Thibodeaux, L. J. and J. D. Boyle (1987), Bedform-generated convective transport in bottom sediment, *Nature*, 325(22), 341-343.

Trauth, N., C. Schmidth, U. Maier, M. Wieweg, and J. H. Fleckenstein (2013), Coupled 3-D stream flow and hyporheic flow model under vary- ing stream and ambient groundwater flow conditions in a pool-riffle system, *Water Resour. Res.*, 49,

5834–5850, doi:10.1002/wrcr.20442.

Trauth, N., J. C. Schmidt, M. Vieweg, U. Maier, and J. H. Fleckenstein (2014), Hyporheic transport and biogeochemical reactions in pool-riffle systems under varying ambient groundwater flow conditions, *J. Geophys. Res. Biogeosci.*, 119, 910–928, doi:10.1002/2013JG002586.

United States Environmental Protection Agency (2017), U. S. Environmental Protection Agency. [online] Available at: http://www.citethisforme.com/guides/harvard/how-to-cite-a-website [Accessed 30 May, 2017].

Vaux, W. G. (1968), Intragravel flow and interchange of water in streambed, *Fishery Bulletin,* 66.

Yalin, M. S. (1964), Geometrical properties of sand waves, *J. Hydraul. Div.-ASCE*, *90*(5), 105–119.

Yates, M. V., C. P. Gerba and L. M. Kelley (1985), Virus persistence in groundwater, *Applied and environmental microbiology*, 778-781.

Zarnetske, J. P., R. Haggerty, S. M. Wondzell, and M. A. Baker (2011), Dynamics of nitrate production and removal as a function of residence time in the hyporheic zone, *J. Geophys. Res.*, 116, G01025, doi:10.1029/2010JG001356.

Zarnetske, J. P., R. Haggerty, S. M. Wondzell, V. A. Bokil, and R. Gonzalez-Pinzon (2012), Coupled transport and reaction kinetics control the nitrate source-sink function of hyporheic zones, *Water Resour. Res.*, 48, W11508, doi:10.1029/2012WR011894.

Zuur, A. F., E. N. Ieno and C. S. Elphick (2010), A protocol for data exploration to avoid common statistical problems. *Method. Ecol. Evol.*, *1,* 3-14.

Appendices

A. Uptake velocity of oxygen Mathematica code

Computing RTDs from the Analytical Solution

Calculation involves 5 steps.

Step 1: Parameter definition (user must specify values for the following parameters which apply for all the model)

(a) qvbar= the normalized vertical groundwater Darcy flux (-)
(b) theta=porosity (-)
(c) z0=depth of mineralization decay (m)

```
Clear[qvbar]; qvbar = 0;
Clear[theta]; theta = 0.32;
Clear[z0]; z0 = 0.1;
```

Step 2 : Assign parameter values (chemical + physical) specific to each LINXII site

(a) qubar = the normalized horizontal groundwater Darcy flux (–)
(b) qH0 = Characteristic hyporheic exchange flux (m / s)
(c) tT = Characteristic residecne time (s)
(d) cO20 = in – stream concentration of oxygen (mol / m3)
(e) cNH40 = in – stream concentration of ammonium (mol / m3)
(f) KO2sat = half – saturation constant for oxygen (mol / m3)
(g) ER = ecosystem respiration (mol / m2 / s)
(h) kNI = nitrification rate constant (m3 / mol / s)

Kimball

```
Clear[qubar]; qubar = 4.34 * 10^-04;
Clear[qH0]; qH0 = 1.12 * 10^-03;
Clear[tT]; tT = 1.87 * 10^+01;
Clear[cO20]; cO20 = 1.68 * 10^-01;
Clear[cNH40]; cNH40 = 7.14 * 10^-05;
Clear[kO2Sat]; kO2Sat = 6 * 10^-3;
Clear[ER]; ER = 4.34 * 10^-06;
Clear[kNI]; kNI = 10^-2.67;
```

Bernalillo drain

```
Clear[qubar]; qubar = 1.12 * 10^-03;
Clear[qH0]; qH0 = 1.75 * 10^-04;
Clear[tT]; tT = 9.66 * 10^+01;
Clear[cO20]; cO20 = 1.87 * 10^-01;
Clear[cNH40]; cNH40 = 1.43 * 10^-04;
Clear[kO2Sat]; kO2Sat = 6 * 10^-3;
Clear[ER]; ER = 2.53 * 10^-06;
Clear[kNI]; kNI = 10^-2.67;
```

Rio Rancho

```
Clear[qubar]; qubar = 1.43 * 10^-03;
Clear[qH0]; qH0 = 9.21 * 10^-05;
Clear[tT]; tT = 1.28 * 10^+02;
Clear[cO20]; cO20 = 1.84 * 10^-01;
Clear[cNH40]; cNH40 = 2.14 * 10^-04;
Clear[kO2Sat]; kO2Sat = 6 * 10^-3;
Clear[ER]; ER = 3.62 * 10^-06;
Clear[kNI]; kNI = 10^-2.67;
```

Giltner

```
Clear[qubar]; qubar = 2.28 * 10^-04;
Clear[qH0]; qH0 = 1.78 * 10^-03;
Clear[tT]; tT = 8.95 * 10^+00;
Clear[cO20]; cO20 = 9.64 * 10^-01;
Clear[cNH40]; cNH40 = 2.14 * 10^-04;
Clear[kO2Sat]; kO2Sat = 6 * 10^-3;
Clear[ER]; ER = 4.12 * 10^-06;
Clear[kNI]; kNI = 10^-2.67;
```

Headquarters

```
Clear[qubar]; qubar = 1.86 * 10^-04;
Clear[qH0]; qH0 = 1.63 * 10^-03;
Clear[tT]; tT = 9.38 * 10^+00;
Clear[cO20]; cO20 = 1.81 * 10^-01;
Clear[cNH40]; cNH40 = 2.14 * 10^-04;
Clear[kO2Sat]; kO2Sat = 6 * 10^-3;
Clear[ER]; ER = 2.57 * 10^-06;
Clear[kNI]; kNI = 10^-2.67;
```

Bullet

```
Clear[qubar]; qubar = 3.44 * 10^-04;
Clear[qH0]; qH0 = 2.86 * 10^-03;
Clear[tT]; tT = 1.61 * 10^+00;
Clear[cO20]; cO20 = 3.11 * 10^-01;
Clear[cNH40]; cNH40 = 7.86 * 10^-04;
Clear[kO2Sat]; kO2Sat = 6 * 10^-3;
Clear[ER]; ER = 5.64 * 10^-06;
Clear[kNI]; kNI = 10^-2.67;
```

Honeysuckle

```
Clear[qubar]; qubar = 2.34 * 10^-04;
Clear[qH0]; qH0 = 3.24 * 10^-03;
Clear[tT]; tT = 4.82 * 10^+00;
Clear[cO20]; cO20 = 2.75 * 10^-01;
Clear[cNH40]; cNH40 = 1.50 * 10^-03;
Clear[kO2Sat]; kO2Sat = 6 * 10^-3;
Clear[ER]; ER = 2.86 * 10^-06;
Clear[kNI]; kNI = 10^-2.67;
```

Black Brook

```
Clear[qubar]; qubar = 3.60 * 10^-02;
Clear[qH0]; qH0 = 2.18 * 10^-05;
Clear[tT]; tT = 4.94 * 10^+03;
Clear[cO20]; cO20 = 1.20 * 10^-01;
Clear[cNH40]; cNH40 = 2.21 * 10^-03;
Clear[kO2Sat]; kO2Sat = 6 * 10^-3;
Clear[ER]; ER = 1.63 * 10^-06;
Clear[kNI]; kNI = 10^-2.67;
```

Arcadia

```
Clear[qubar]; qubar = 4.64 * 10^-05;
Clear[qH0]; qH0 = 1.51 * 10^-03;
Clear[tT]; tT = 1.69 * 10^+01;
Clear[cO20]; cO20 = 2.05 * 10^-01;
Clear[cNH40]; cNH40 = 2.29 * 10^-03;
Clear[kO2Sat]; kO2Sat = 6 * 10^-3;
Clear[ER]; ER = 5.10 * 10^-06;
Clear[kNI]; kNI = 10^-2.67;
```

IS_118

```
Clear[qubar]; qubar = 7.70 * 10^-04;
Clear[qH0]; qH0 = 1.31 * 10^-05;
Clear[tT]; tT = 1.01 * 10^+03;
Clear[cO20]; cO20 = 2.32 * 10^-01;
Clear[cNH40]; cNH40 = 2.79 * 10^-03;
Clear[kO2Sat]; kO2Sat = 6 * 10^-3;
Clear[ER]; ER = 1.45 * 10^-06;
Clear[kNI]; kNI = 10^-2.67;
```

Sand Creek

```
Clear[qubar]; qubar = 2.58 * 10^-04;
Clear[qH0]; qH0 = 4.36 * 10^-03;
Clear[tT]; tT = 8.90 * 10^-01;
Clear[cO20]; cO20 = 2.74 * 10^-01;
Clear[cNH40]; cNH40 = 3.93 * 10^-03;
Clear[kO2Sat]; kO2Sat = 6 * 10^-3;
Clear[ER]; ER = 7.23 * 10^-07;
Clear[kNI]; kNI = 10^-2.67;
```

Long Meadow Brook

```
Clear[qubar]; qubar = 4.45 * 10^-05;
Clear[qH0]; qH0 = 2.27 * 10^-04;
Clear[tT]; tT = 2.55 * 10^+01;
Clear[cO20]; cO20 = 2.24 * 10^-01;
Clear[cNH40]; cNH40 = 4.50 * 10^-03;
Clear[kO2Sat]; kO2Sat = 6 * 10^-3;
Clear[ER]; ER = 2.96586 * 10^-06;
Clear[kNI]; kNI = 10^-2.67;
```

Wayland

```
Clear[qubar]; qubar = 2.47 * 10^-04;
Clear[qH0]; qH0 = 2.27 * 10^-03;
Clear[tT]; tT = 3.58 * 10^+00;
Clear[cO20]; cO20 = 2.41 * 10^-01;
Clear[cNH40]; cNH40 = 5.29 * 10^-03;
Clear[kO2Sat]; kO2Sat = 6 * 10^-3;
Clear[ER]; ER = 2.53 * 10^-06;
Clear[kNI]; kNI = 10^-2.67;
```

Runaway Brook

```
Clear[qubar]; qubar = 1.90 * 10^-04;
Clear[qH0]; qH0 = 5.31 * 10^-05;
Clear[tT]; tT = 1.16 * 10^+02;
Clear[cO20]; cO20 = 2.66 * 10^-01;
Clear[cNH40]; cNH40 = 5.71 * 10^-03;
Clear[kO2Sat]; kO2Sat = 6 * 10^-3;
Clear[ER]; ER = 1.6276 * 10^-06;
Clear[kNI]; kNI = 10^-2.67;
```

Jerry Branch

```
Clear[qubar]; qubar = 3.40 * 10^-04;
Clear[qH0]; qH0 = 3.30 * 10^-03;
Clear[tT]; tT = 2.86 * 10^+00;
Clear[cO20]; cO20 = 2.39 * 10^-01;
Clear[cNH40]; cNH40 = 7.71 * 10^-03;
Clear[kO2Sat]; kO2Sat = 6 * 10^-3;
Clear[ER]; ER = 1.6276 * 10^-06;
Clear[kNI]; kNI = 10^-2.67;
```

IS_104

```
Clear[qubar]; qubar = 4.82 * 10^-04;
Clear[qH0]; qH0 = 2.10 * 10^-05;
Clear[tT]; tT = 4.98 * 10^+02;
Clear[cO20]; cO20 = 1.59 * 10^-01;
Clear[cNH40]; cNH40 = 8.64 * 10^-03;
Clear[kO2Sat]; kO2Sat = 6 * 10^-3;
Clear[ER]; ER = 3.29138 * 10^-06;
Clear[kNI]; kNI = 10^-2.67;
```

DORR

```
Clear[qubar]; qubar = 4.27 * 10^-04;
Clear[qH0]; qH0 = 1.64 * 10^-03;
Clear[tT]; tT = 1.03 * 10^+01;
Clear[cO20]; cO20 = 2.15 * 10^-01;
Clear[cNH40]; cNH40 = 9.14 * 10^-03;
Clear[kO2Sat]; kO2Sat = 6 * 10^-3;
Clear[ER]; ER = 3.1467 * 10^-06;
Clear[kNI]; kNI = 10^-2.67;
```

Sawmill Brook

```
Clear[qubar]; qubar = 1.43 * 10^-03;
Clear[qH0]; qH0 = 1.04 * 10^-03;
Clear[tT]; tT = 9.08 * 10^+00;
Clear[cO20]; cO20 = 2.33 * 10^-01;
Clear[cNH40]; cNH40 = 1.81 * 10^-02;
Clear[kO2Sat]; kO2Sat = 6 * 10^-3;
Clear[ER]; ER = 4.34028 * 10^-07;
Clear[kNI]; kNI = 10^-2.67;
```

Gravelly Brook

```
Clear[qubar]; qubar = 5.62 * 10^-03;
Clear[qH0]; qH0 = 1.07 * 10^-04;
Clear[tT]; tT = 3.95 * 10^+01;
Clear[cO20]; cO20 = 9.35 * 10^-02;
Clear[cNH40]; cNH40 = 3.11 * 10^-02;
Clear[kO2Sat]; kO2Sat = 6 * 10^-3;
Clear[ER]; ER = 4.08709 * 10^-06;
Clear[kNI]; kNI = 10^-2.67;
```

Step 3: Define variables and functions

*F1 and F2 are the CDFs for the upstream and downstream flow cells.
*end (returned by the function "endtime") is the normalized travel time along a streamline through the hyporheic zone with a particular starting position x0val along the sediment-water interface (see description in Section 5.2.1 of the main text).
*frtdupmax and frtddnmax are the maximum fractions of the hyporheic flux circulating through the upstream and downstream flow cells, respectively (note that these fractions should add to unity).
*xbarsep (returned by the function "xbarsepfunc") is the normalized x - coordinate where the streamline separating the upstream and downstream flow cells intersects the sediment-water interface.
*abar is the normalized x - coordinate separating upwelling and downwelling regions in the upstream flow cell
*bbar is the normalized x - coordinate separating upwelling and downwelling regions in the downstream flow cell
*f1func returns the fraction of the hyporheic exchange flux flowing through the upstream flow cell that has starting streamlines between x0bar and abar.
*f2func returns the fraction of the hyporheic exchange flux flowing through the downstream flow cell that has starting streamlines between x0bar and bbar.
*x0valup is the normalized x - coordinate at the sediment-water interface returned by x0valuesup, denoting the streamline starting position associated with a given value of F1
*x0valdn is the normalized x - coordinate at the sediment-water interface returned by x0valuesdn, denoting the streamline starting position associated

with a given value of F2

```
(*compute the x-coordinate where the separation
  streamline intersects the sediment-water interface*)
Clear[xbarsepfunc];
xbarsepfunc := FindRoot[Cos[xbarsep] + qvbar xbarsep ==
    Cos[ArcTan[qvbar / qubar]] Sqrt[qubar^2 + qvbar^2] + qvbar ArcTan[qvbar / qubar] -
     qubar Log[Sqrt[qubar^2 + qvbar^2]], {xbarsep, Pi / 2}]
(*compute the x-coordinate separating upwelling and
  downwelling zones in the upstream flow cell*)
Clear[abar]; abar = ArcSin[qvbar];
(*compute the x-coordinate separating upwelling
  and downwelling zones in the downstream flow cell*)
Clear[bbar]; bbar = Pi - ArcSin[qvbar];
(*compute the fraction of flow circulating through the upstream flow
 cell downwelling between abar and x0bar; this is equal to F1(xobar)*)
Clear[f1func];
f1func[x0bar_] :=
 (Abs[qvbar] (x0bar - ArcSin[Abs[qvbar]]) - Sqrt[1 - Abs[qvbar]^2] + Cos[x0bar]) /
  (2 (Abs[qvbar] (Pi / 2 - ArcSin[Abs[qvbar]]) - Sqrt[1 - Abs[qvbar]^2]));
(*compute the fraction of flow circulating through the downstream flow
 cell downwelling between x0bar and bbar; this is equal to F2(xobar)*)
Clear[f2func];
f2func[x0bar_] :=
 (Abs[qvbar] (Pi - x0bar - ArcSin[Abs[qvbar]]) - Sqrt[1 - Abs[qvbar]^2] - Cos[x0bar]) /
  (2 (Abs[qvbar] (Pi / 2 - ArcSin[Abs[qvbar]]) - Sqrt[1 - Abs[qvbar]^2]));
(*compute the fraction of the hyporheic exchange flux
 associated with the upstream flow cell*)
Clear[frtdupmax]; frtdupmax = f1func[xbarsep /. xbarsepfunc];
(*compute the fraction of the hyporheic
 exchange flux associated with the downstream flow cell*)
Clear[frtddnmax]; frtddnmax = f2func[xbarsep /. xbarsepfunc];
(*compute the streamline starting position
 in the upstream flow cell for a given F1 value*)
Clear[x0valuesup, f1val];
x0valuesup[xbarsep_, f1val_] := FindRoot[Abs[qvbar] x0valup + Cos[x0valup] ==
    2 f1val (Abs[qvbar] (Pi / 2 - ArcSin[qvbar]) - Sqrt[1 - Abs[qvbar]^2]) + Sqrt[1 -
       Abs[qvbar]^2] + Abs[qvbar] ArcSin[Abs[qvbar]], {x0valup, (abar + xbarsep) / 2}];
(*compute the streamline starting position in the downstream
 flow cell for a given F2 value *)
Clear[x0valuesdn, f2val];
x0valuesdn[xbarsep_, f2val_] := FindRoot[Abs[qvbar] x0valdn + Cos[x0valdn] ==
    -2 f2val (Abs[qvbar] (Pi / 2 - ArcSin[qvbar]) - Sqrt[1 - Abs[qvbar]^2]) -
     Sqrt[1 - Abs[qvbar]^2] + Abs[qvbar] (Pi - ArcSin[Abs[qvbar]]),
```

```
  {x0valdn, (bbar + xbarsep) / 2}];
(*compute the travel time associated with the streamline in either
 the upstream or downstream flow cell that starts at x0bar;
the travel time is returned as "end"*)
Clear[endtime];
endtime[x0bar_] :=
 NDSolve[{(1 / 2.303) x'[u] == -(10^u) Cos[x[u]] Exp[y[u]] + (10^u) qubar,
    (1 / 2.303) y'[u] == -(10^u) Sin[x[u]] Exp[y[u]] + (10^u) qvbar, x[-5] == x0bar,
    y[-5] == 0, WhenEvent[y[u] > 0, {end = u, "StopIntegration"}]}, {x, y}, {u, -5, 5}];
```

Step 4: Prepare probability distributions for residence times in the upstream and downstream flow cells (note this step will take a few moments to complete)

*Dup and Ddn are the probability distributions constructed from 10,000 realizations of the FRTDs associated with the upstream and downstream flow cells, respectively.

```
Clear[𝒟up];
𝒟up = SmoothKernelDistribution[Table[Clear[a, b, x0valup, xbarsep];
    a = RandomReal[];
    b = x0valup /. x0valuesup[xbarsep /. xbarsepfunc, Evaluate[a frtdupmax]];
    end /. First[endtime[b]], {i, 1, 10 000}], 0.1];
Clear[𝒟dn];
𝒟dn = SmoothKernelDistribution[Table[Clear[a, b, x0valdn, xbarsep];
    a = RandomReal[];
    b = x0valdn /. x0valuesdn[xbarsep /. xbarsepfunc, Evaluate[a frtddnmax]];
    end /. First[endtime[b]], {i, 1, 10 000}], 0.1];
```

Step 5: Plot results and check output

```
(*check to make sure that the total probability associated with the
 upstream and downstream flow cells sum to unity*)frtdupmax + frtddnmax == 1
(*plot the upstream, downstream, and total RTD PDFs*)
Plot[{frtdupmax CDF[𝒟up, x], frtddnmax CDF[𝒟dn, x],
   frtdupmax CDF[𝒟up, x] + frtddnmax CDF[𝒟dn, x]}, {x, -1, 3},
 PlotLabels → {"upstream cell", "downstream cell", "total"},
 AxesLabel → {"log10(taubar)", "F1,F2, or FRTD"},
 PlotStyle → {Blue, Orange, Green}, PlotLabel → CDF]
Plot[{frtdupmax PDF[𝒟up, x], frtddnmax PDF[𝒟dn, x],
   frtdupmax PDF[𝒟up, x] + frtddnmax PDF[𝒟dn, x]},
 {x, -1, 3}, AxesLabel → {"log10(taubar)", "dFRTD/dlog10(tau)"},
 PlotStyle → {Blue, Orange, Green}, PlotLabel → PDF]
```

```
True
```

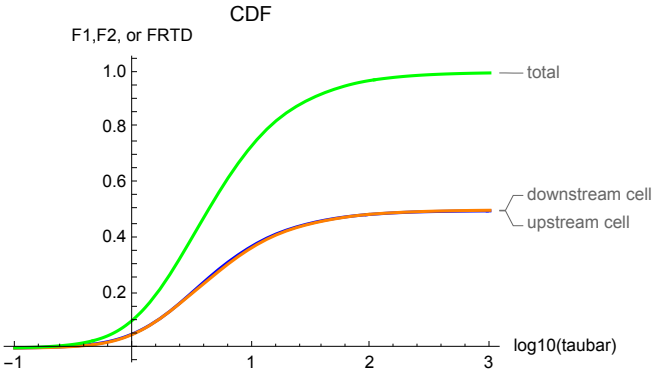

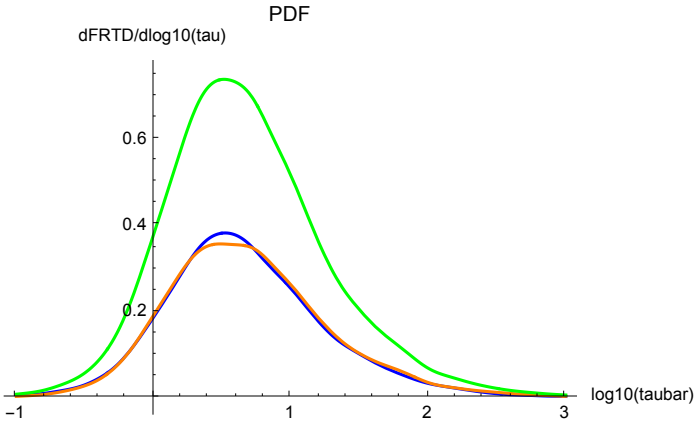

Computing Chemistry Solution

Calculation involves 4 steps.

Step 1: Calculate parameters derived from the parameter values

(a) lrmin0 = mineralization constant in log-scale (mol/m3/s).
(b) tr = Respiration time scale (taur, units s).
(c) delta = relative rates of nitrification and respiration (-).
(d) Normalized aerobic saturation constant (kO2SatHat, unitless).
(e) Uptake velocity of oxygen calculated from LINXII data.
(f) alpha = normalized ammonium concentration (-).

```
Clear[lrmin0]; lrmin0 = 3.0411 + 1.2571 * Log[10, ER];
Clear[tr]; tr = kO2Sat / (10^lrmin0);
Clear[delta]; delta = tr kNI cO20;
Clear[kO2SatHat]; kO2SatHat = kO2Sat / cO20;
Clear[vfO2exp]; vfO2exp = -ER / cO20
Clear[alpha]; alpha = cNH40 / cO20;
```

Step 2: Solve the mass balance equations

The following equation is expression of mass balance for the concentrations of oxygen (cO2) normalized by in-stream oxygen concentration as a function of non-dimensional travel time (taur=tau/tr) through the hyporheic zone. To solve these equations, user must define the ending time of the simulation (endtime=log10taur). Note that the starting time is assumed to be taur=10^-10, while the integral stops integrating when the oxygen concentration falls below 10^-5 of the in-stream oxygen concentration.

```
Clear[kO2Satvar, deltavar, alphavar, cO2, cNH4, soln, end];
soln[kO2Satvar_, deltavar_, alphavar_] :=
 NDSolve[{(1 / 2.303) cO2'[u] == (10^u) (-Exp[-((qH0 * tr * 10^u) / (theta * z0))^2] *
         (cO2[u] / (cO2[u] / kO2Satvar + 1)) - 2 deltavar cO2[u] cNH4[u]),
   cO2[-10] == 1, (1 / 2.303) cNH4'[u] == (10^u) (-deltavar cO2[u] cNH4[u]),
   cNH4[-10] == alphavar, WhenEvent[cO2[u] < 10^-5, {end = u, "StopIntegration"}]},
  {cO2, cNH4}, {u, -10, 10}]
```

Step 3: Plot the oxygen concentration versus non–dimensional (tau/tr) travel time through the hyporheic zone.

```
Clear[sn]; sn = soln[kO2SatHat, delta, alpha];
LogPlot[{cO2[u] /. sn, (cNH4[u] / alpha) /. sn}, {u, -10, 10}, PlotRange → {.00001, 10},
 AxesLabel → {"log10(tau/tr)", "C_HZ/C_Stream"}, PlotStyle → {Blue, Orange},
 PlotLabels → Placed[{"oxygen", "ammonium"}, {Scaled[1], Before}]]
```

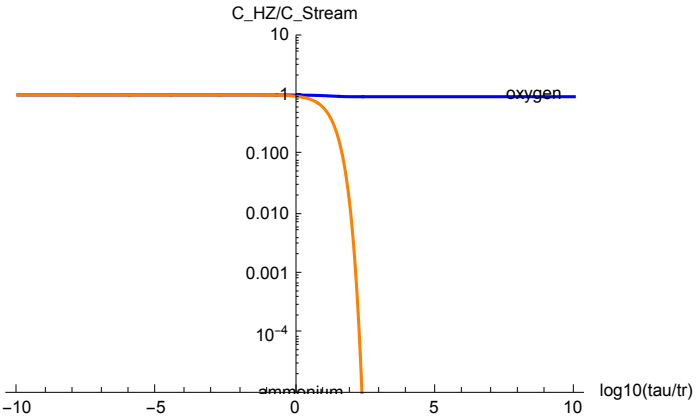

Step 4: Calculate vfO2

```
vfO2 = (qH0 * (NIntegrate[(cO2[u + Log10[tT / tr]] /. sn)
        (frtdupmax PDF[𝒟up, u] + frtddnmax PDF[𝒟dn, u]), {u, -10 - Log10[tT / tr],
        10 - Log10[tT / tr]}, WorkingPrecision → 10, MinRecursion → 1] - 1))
```

B. Direct denitrification uptake velocity Mathematica code

Computing RTDs from the Analytical Solution

Calculation involves 5 steps.

Step 1: Parameter definition (user must specify values for the following parameters which apply to all the scenarios)

(a) qvbar= the normalized vertical groundwater Darcy flux (-)
(b) theta=porosity (-)
(c) z0=depth of mineralization decay (m)
(d) KO2sat = half-saturation constant for oxygen (mol/m^3)
(e) KNO3sat = half-saturation constant for nitrate (mol/m^3)
(f) KO2inh = Inhibition coefficient for denitrification (mol/m^3)

```
Clear[qvbar]; qvbar = 0;
Clear[theta]; theta = 0.32;
Clear[z0]; z0 = 0.1;
Clear[kO2Sat]; kO2Sat = 6 * 10^-3;
Clear[kNO3Sat]; kNO3Sat = 0.081;
Clear[kO2Inh]; kO2Inh = 3 * 10^-3;
```

Step 2: Assign parameter values (chemical + physical) specific to each LINXII site

(a) qubar = the normalized horizontal groundwater Darcy flux (-)
(b) qH0 = Characteristic hyporheic exchange flux (m/s)
(c) tT = Characteristic residence time (s)
(d) cO20 = in-stream concentration of oxygen (mol/m^3)
(e) cNO30 = in-stream concentration of nitrate (mol/m^3)
(f) cNH40 = in-stream concentration of ammonium (mol/m^3)
(g) ER = ecosystem respiration (mol/m^2/s)
(h) GPP = gross primary production (mol/m^2/s)

Kimball

```
Clear[qubar]; qubar = 4.34 * 10^-04;
Clear[qH0]; qH0 = 1.12 * 10^-03;
Clear[tT]; tT = 1.87 * 10^+01;
Clear[cO20]; cO20 = 1.68 * 10^-01;
Clear[cNO30]; cNO30 = 0.002;
Clear[cNH40]; cNH40 = 7.14 * 10^-5;
Clear[ER]; ER = 4.34 * 10^-06;
Clear[GPP]; GPP = 4.92 * 10^-06;
```

Bernalillo Drain

```
Clear[qubar]; qubar = 1.12 * 10^-03;
Clear[qH0]; qH0 = 1.75 * 10^-04;
Clear[tT]; tT = 9.66 * 10^+01;
Clear[cO20]; cO20 = 1.87 * 10^-01;
Clear[cNO30]; cNO30 = 1.43 * 10^-04;
Clear[cNH40]; cNH40 = 1.43 * 10^-04;
Clear[ER]; ER = 2.53 * 10^-06;
Clear[GPP]; GPP = 3.18 * 10^-06;
```

Rio Rancho

```
Clear[qubar]; qubar = 1.43 * 10^-03;
Clear[qH0]; qH0 = 9.21 * 10^-05;
Clear[tT]; tT = 1.28 * 10^2;
Clear[cO20]; cO20 = 1.84 * 10^-01;
Clear[cNO30]; cNO30 = 9.29 * 10^-04;
Clear[cNH40]; cNH40 = 2.14 * 10^-04;
Clear[ER]; ER = 3.62 * 10^-06;
Clear[GPP]; GPP = 2.35 * 10^-06;
```

Giltner

```
Clear[qubar]; qubar = 2.28 * 10^-04;
Clear[qH0]; qH0 = 1.78 * 10^-03;
Clear[tT]; tT = 8.95 * 10^+00;
Clear[cO20]; cO20 = 9.64 * 10^-01;
Clear[cNO30]; cNO30 = 3.57 * 10^-03;
Clear[cNH40]; cNH40 = 2.14 * 10^-04;
Clear[ER]; ER = 4.12 * 10^-06;
Clear[GPP]; GPP = 5.86 * 10^-06;
```

Headquarters

```
Clear[qubar]; qubar = 1.86 * 10^-04;
Clear[qH0]; qH0 = 1.63 * 10^-03;
Clear[tT]; tT = 9.38 * 10^+00;
Clear[cO20]; cO20 = 1.81 * 10^-01;
Clear[cNO30]; cNO30 = 7.14 * 10^-05;
Clear[cNH40]; cNH40 = 2.14 * 10^-04;
Clear[ER]; ER = 2.57 * 10^-06;
Clear[GPP]; GPP = 1.19 * 10^-06;
```

Bullet

```
Clear[qubar]; qubar = 3.44 * 10^-04;
Clear[qH0]; qH0 = 2.86 * 10^-03;
Clear[tT]; tT = 1.61 * 10^+00;
Clear[cO20]; cO20 = 3.11 * 10^-01;
Clear[cNO30]; cNO30 = 2.74 * 10^-02;
Clear[cNH40]; cNH40 = 7.86 * 10^-4;
Clear[ER]; ER = 5.64 * 10^-06;
Clear[GPP]; GPP = 5.79 * 10^-7;
```

Honeysuckle

```
Clear[qubar]; qubar = 2.34 * 10^-04;
Clear[qH0]; qH0 = 3.24 * 10^-03;
Clear[tT]; tT = 4.82 * 10^+00;
Clear[cO20]; cO20 = 2.75 * 10^-01;
Clear[cNO30]; cNO30 = 2.86 * 10^-04;
Clear[cNH40]; cNH40 = 1.50 * 10^-03;
Clear[ER]; ER = 2.86 * 10^-06;
Clear[GPP]; GPP = 3.62 * 10^-08;
```

Black Brook

```
Clear[qubar]; qubar = 3.60 * 10^-02;
Clear[qH0]; qH0 = 2.18 * 10^-05;
Clear[tT]; tT = 4.94 * 10^03;
Clear[cO20]; cO20 = 1.20 * 10^-01;
Clear[cNO30]; cNO30 = 3.57 * 10^-03;
Clear[cNH40]; cNH40 = 2.21 * 10^-03;
Clear[ER]; ER = 1.63 * 10^-06;
Clear[GPP]; GPP = 2.17 * 10^-07;
```

Arcadia

```
Clear[qubar]; qubar = 4.64 * 10^-05;
Clear[qH0]; qH0 = 1.51 * 10^-03;
Clear[tT]; tT = 1.69 * 10^+01;
Clear[cO20]; cO20 = 2.05 * 10^-01;
Clear[cNO30]; cNO30 = 1.96 * 10^-02;
Clear[cNH40]; cNH40 = 2.29 * 10^-03;
Clear[ER]; ER = 5.10 * 10^-06;
Clear[GPP]; GPP = 2.89 * 10^-07;
```

IS118

```
Clear[qubar]; qubar = 7.70 * 10^-04;
Clear[qH0]; qH0 = 1.31 * 10^-05;
Clear[tT]; tT = 1.01 * 10^03;
Clear[cO20]; cO20 = 2.32 * 10^-01;
Clear[cNO30]; cNO30 = 7.32 * 10^-02;
Clear[cNH40]; cNH40 = 2.79 * 10^-03;
Clear[ER]; ER = 1.45 * 10^-06;
Clear[GPP]; GPP = 3.62 * 10^-08;
```

Sand Creek

```
Clear[qubar]; qubar = 2.58 * 10^-04;
Clear[qH0]; qH0 = 4.36 * 10^-03;
Clear[tT]; tT = 8.90 * 10^-01;
Clear[cO20]; cO20 = 2.74 * 10^-01;
Clear[cNO30]; cNO30 = 2.02 * 10^-02;
Clear[cNH40]; cNH40 = 3.93 * 10^-03;
Clear[ER]; ER = 7.23 * 10^-07;
Clear[GPP]; GPP = 7.23 * 10^-08;
```

Long Meadow Brook

```
Clear[qubar]; qubar = 4.45 * 10^-05;
Clear[qH0]; qH0 = 2.27 * 10^-04;
Clear[tT]; tT = 2.55 * 10^+01;
Clear[cO20]; cO20 = 2.24 * 10^-01;
Clear[cNO30]; cNO30 = 7.06 * 10^-02;
Clear[cNH40]; cNH40 = 4.50 * 10^-03;
Clear[ER]; ER = 2.96586 * 10^-06;
Clear[GPP]; GPP = 1.41 * 10^-06;
```

Wayland

```
Clear[qubar]; qubar = 2.47 * 10^-04;
Clear[qH0]; qH0 = 2.27 * 10^-03;
Clear[tT]; tT = 3.58 * 10^+00;
Clear[cO20]; cO20 = 2.41 * 10^-01;
Clear[cNO30]; cNO30 = 4.96 * 10^-02;
Clear[cNH40]; cNH40 = 5.29 * 10^-03;
Clear[ER]; ER = 1.48293 * 10^-06;
Clear[GPP]; GPP = 6.51 * 10^-07;
```

Runaway Brook

```
Clear[qubar]; qubar = 1.90 * 10^-04;
Clear[qH0]; qH0 = 5.31 * 10^-05;
Clear[tT]; tT = 1.16 * 10 + 02;
Clear[cO20]; cO20 = 2.66 * 10^-01;
Clear[cNO30]; cNO30 = 8.31 * 10^-02;
Clear[cNH40]; cNH40 = 5.71 * 10^-03;
Clear[ER]; ER = 1.6276 * 10^-06;
Clear[GPP]; GPP = 2.64 * 10^-06;
```

Jerry Branch

```
Clear[qubar]; qubar = 3.40 * 10^-04;
Clear[qH0]; qH0 = 3.30 * 10^-03;
Clear[tT]; tT = 2.86 * 10^+00;
Clear[cO20]; cO20 = 2.39 * 10^-01;
Clear[cNO30]; cNO30 = 2.90 * 10^-02;
Clear[cNH40]; cNH40 = 7.71 * 10^-03;
Clear[ER]; ER = 1.6276 * 10^-06;
Clear[GPP]; GPP = 1.81 * 10^-07;
```

Sawmill Brook

```
Clear[qubar]; qubar = 1.43 * 10^-03;
Clear[qH0]; qH0 = 1.04 * 10^-03;
Clear[tT]; tT = 9.08 * 10^+00;
Clear[cO20]; cO20 = 2.33 * 10^-01;
Clear[cNO30]; cNO30 = 3.66 * 10^-02;
Clear[cNH40]; cNH40 = 1.81 * 10^-02;
Clear[ER]; ER = 4.34028 * 10^-07;
Clear[GPP]; GPP = 1.81 * 10^-08;
```

IS104

```
Clear[qubar]; qubar = 4.82 * 10^-04;
Clear[qH0]; qH0 = 2.10 * 10^-05;
Clear[tT]; tT = 4.98 * 10^+02;
Clear[cO20]; cO20 = 1.59 * 10^-01;
Clear[cNO30]; cNO30 = 9.54 * 10^-02;
Clear[cNH40]; cNH40 = 8.64 * 10^-03;
Clear[ER]; ER = 3.29 * 10^-06;
Clear[GPP]; GPP = 2.53 * 10^-07;
```

DORR

```
Clear[qubar]; qubar = 4.27 * 10^-04;
Clear[qH0]; qH0 = 1.64 * 10^-03;
Clear[tT]; tT = 1.03 * 10^+01;
Clear[cO20]; cO20 = 2.15 * 10^-01;
Clear[cNO30]; cNO30 = 7.86 * 10^-02;
Clear[cNH40]; cNH40 = 9.14 * 10^-03;
Clear[ER]; ER = 3.15 * 10^-06;
Clear[GPP]; GPP = 2.53 * 10^-07;
```

Step 3: Define variables and functions

*F1 and F2 are the CDFs for the upstream and downstream flow cells.
*end (returned by the function "endtime") is the normalized travel time along a streamline through the hyporheic zone with a particular starting position x0val along the sediment-water interface (see description in Section 5.2.1 of the main text).
*frtdupmax and frtddnmax are the maximum fractions of the hyporheic flux circulating through the upstream and downstream flow cells, respectively (note that these fractions should add to unity).
*xbarsep (returned by the function "xbarsepfunc") is the normalized x - coordinate where the streamline separating the upstream and downstream flow cells intersects the sediment-water interface.
*abar is the normalized x - coordinate separating upwelling and downwelling regions in the upstream flow cell
*bbar is the normalized x - coordinate separating upwelling and downwelling regions in the downstream flow cell
*f1func returns the fraction of the hyporheic exchange flux flowing through the upstream flow cell that has starting streamlines between x0bar and abar.
*f2func returns the fraction of the hyporheic exchange flux flowing through the downstream flow cell that has starting streamlines between x0bar and bbar.
*x0valup is the normalized x - coordinate at the sediment-water interface returned by x0valuesup, denoting the streamline starting position associated with a given value of F1
*x0valdn is the normalized x - coordinate at the sediment-water interface returned by x0valuesdn, denoting the streamline starting position associated with a given value of F2

```
(*compute the x-coordinate where the separation
  streamline intersects the sediment-water interface*)
Clear[xbarsepfunc];
xbarsepfunc := FindRoot[Cos[xbarsep] + qvbar xbarsep ==
   Cos[ArcTan[qvbar / qubar]] Sqrt[qubar^2 + qvbar^2] + qvbar ArcTan[qvbar / qubar] -
    qubar Log[Sqrt[qubar^2 + qvbar^2]], {xbarsep, Pi / 2}]
(*compute the x-coordinate separating upwelling and
  downwelling zones in the upstream flow cell*)
```

```
Clear[abar]; abar = ArcSin[qvbar];
(*compute the x-coordinate separating upwelling
  and downwelling zones in the downstream flow cell*)
Clear[bbar]; bbar = Pi - ArcSin[qvbar];
(*compute the fraction of flow circulating through the upstream flow
 cell downwelling between abar and x0bar; this is equal to F1(xobar)*)
Clear[f1func];
f1func[x0bar_] :=
 (Abs[qvbar] (x0bar - ArcSin[Abs[qvbar]]) - Sqrt[1 - Abs[qvbar]^2] + Cos[x0bar]) /
  (2 (Abs[qvbar] (Pi / 2 - ArcSin[Abs[qvbar]]) - Sqrt[1 - Abs[qvbar]^2]));
(*compute the fraction of flow circulating through the downstream flow
 cell downwelling between x0bar and bbar; this is equal to F2(xobar)*)
Clear[f2func];
f2func[x0bar_] :=
 (Abs[qvbar] (Pi - x0bar - ArcSin[Abs[qvbar]]) - Sqrt[1 - Abs[qvbar]^2] - Cos[x0bar]) /
  (2 (Abs[qvbar] (Pi / 2 - ArcSin[Abs[qvbar]]) - Sqrt[1 - Abs[qvbar]^2]));
(*compute the fraction of the hyporheic exchange flux
 associated with the upstream flow cell*)
Clear[frtdupmax]; frtdupmax = f1func[xbarsep /. xbarsepfunc];
(*compute the fraction of the hyporheic
 exchange flux associated with the downstream flow cell*)
Clear[frtddnmax]; frtddnmax = f2func[xbarsep /. xbarsepfunc];
(*compute the streamline starting position
 in the upstream flow cell for a given F1 value*)
Clear[x0valuesup, f1val];
x0valuesup[xbarsep_, f1val_] := FindRoot[Abs[qvbar] x0valup + Cos[x0valup] ==
   2 f1val (Abs[qvbar] (Pi / 2 - ArcSin[qvbar]) - Sqrt[1 - Abs[qvbar]^2]) + Sqrt[1 -
      Abs[qvbar]^2] + Abs[qvbar] ArcSin[Abs[qvbar]], {x0valup, (abar + xbarsep) / 2}];
(*compute the streamline starting position in the downstream
 flow cell for a given F2 value *)
Clear[x0valuesdn, f2val];
x0valuesdn[xbarsep_, f2val_] := FindRoot[Abs[qvbar] x0valdn + Cos[x0valdn] ==
   -2 f2val (Abs[qvbar] (Pi / 2 - ArcSin[qvbar]) - Sqrt[1 - Abs[qvbar]^2]) -
    Sqrt[1 - Abs[qvbar]^2] + Abs[qvbar] (Pi - ArcSin[Abs[qvbar]]),
  {x0valdn, (bbar + xbarsep) / 2}];
(*compute the travel time associated with the streamline in either
 the upstream or downstream flow cell that starts at x0bar;
the travel time is returned as "end"*)
Clear[endtime];
endtime[x0bar_] :=
 NDSolve[{(1 / 2.303) x'[u] == -(10^u) Cos[x[u]] Exp[y[u]] + (10^u) qubar,
   (1 / 2.303) y'[u] == -(10^u) Sin[x[u]] Exp[y[u]] + (10^u) qvbar, x[-5] == x0bar,
   y[-5] == 0, WhenEvent[y[u] > 0, {end = u, "StopIntegration"}]}, {x, y}, {u, -5, 5}];
```

Step 4: Prepare probability distributions for residence times in the upstream and downstream flow cells (note this step will take a few moments to complete)

*Dup and Ddn are the probability distributions constructed from 10,000 realizations of the FRTDs associated with the upstream and downstream flow cells, respectively.

```
Clear[𝒟up];
𝒟up = SmoothKernelDistribution[Table[Clear[a, b, x0valup, xbarsep];
    a = RandomReal[];
    b = x0valup /. x0valuesup[xbarsep /. xbarsepfunc, Evaluate[a frtdupmax]];
    end /. First[endtime[b]], {i, 1, 10 000}], 0.1];
Clear[𝒟dn];
𝒟dn = SmoothKernelDistribution[Table[Clear[a, b, x0valdn, xbarsep];
    a = RandomReal[];
    b = x0valdn /. x0valuesdn[xbarsep /. xbarsepfunc, Evaluate[a frtddnmax]];
    end /. First[endtime[b]], {i, 1, 10 000}], 0.1];
```

Step 5: Plot results and check output

```
(*check to make sure that the total probability associated with the
 upstream and downstream flow cells sum to unity*)frtdupmax + frtddnmax == 1
(*plot the upstream, downstream, and total RTD PDFs*)
Plot[{frtdupmax CDF[𝒟up, x], frtddnmax CDF[𝒟dn, x],
  frtdupmax CDF[𝒟up, x] + frtddnmax CDF[𝒟dn, x]}, {x, -1, 3},
 PlotLabels → {"upstream cell", "downstream cell", "total"},
 AxesLabel → {"log10(taubar)", "F1,F2, or FRTD"},
 PlotStyle → {Blue, Orange, Green}, PlotLabel → CDF]
Plot[{frtdupmax PDF[𝒟up, x], frtddnmax PDF[𝒟dn, x],
  frtdupmax PDF[𝒟up, x] + frtddnmax PDF[𝒟dn, x]},
 {x, -1, 3}, AxesLabel → {"log10(taubar)", "dFRTD/dlog10(tau)"},
 PlotStyle → {Blue, Orange, Green}, PlotLabel → PDF]
```

```
True
```

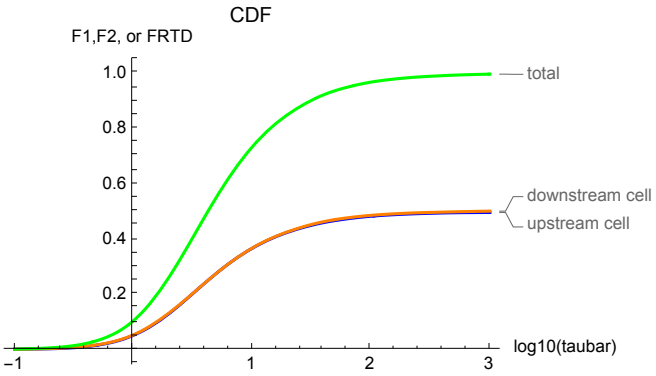

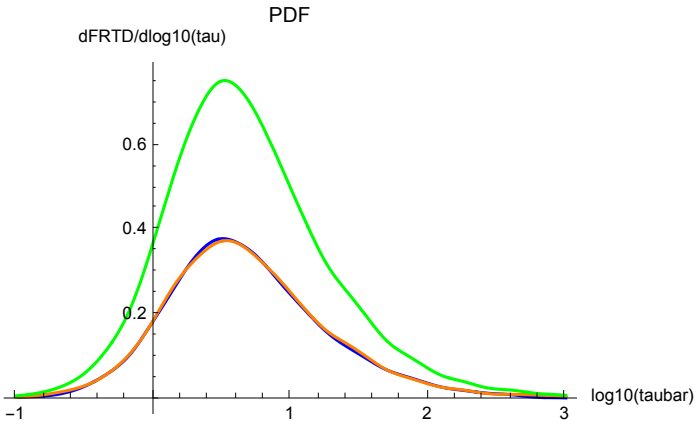

Computing Chemistry Solution

Calculation involves 4 steps.

Step 1: Calculate parameters derived from the parameter values

(a) kNI = nitrification rate constant (m3/mol/s).
(b) rmin0= mineralization constant (mol/m3/s).
(c) Respiration time scale (taur, units s).
(d) delta = relative rates of nitrification and respiration (-).
(e) Normalized aerobic saturation constant (kO2SatHat, unitless).
(f) Normalized denitrification saturation constant (kNO3SatHat, unitless).
(g) Normalized Inhibition constant (kNO2InhHat, unitless).
(h) alpha = normalized ammonium concentration (-).
(i) beta = normalized nitrate concentration (-).
(j) kappa = ratio of denitrified organic carbon molecules to nitrate molecules (unitless).

```
Clear[kNI]; kNI = 10^-2.67
Clear[rmin0]; rmin0 = 10^(3.0411 + 1.2571 * Log10[ER])
Clear[tr]; tr = kO2Sat / (rmin0)
Clear[delta]; delta = tr kNI cO20
Clear[kO2SatHat]; kO2SatHat = kO2Sat / cO20
Clear[kNO3SatHat]; kNO3SatHat = kNO3Sat / cO20
Clear[kO2InhHat]; kO2InhHat = kO2Inh / cO20
Clear[alpha]; alpha = cNH40 / cO20
Clear[beta]; beta = cNO30 / cO20
Clear[kappa]; kappa = 10^(-6.30 - 1.00 * Log10[GPP])
```

Step 2: Solve the mass balance equations (no ammonification)

The following equation is expression of mass balance for the concentrations of oxygen (cO2), ammonium (cNH4), and nitrate (in stream: cNO3, and generated from in-stream ammonium cNO3N), and nitrogen gas generated from in-stream nitrate (cN2) and in-stream nitrified ammonium (cN2N) normalized by in-stream oxygen concentration as a function of non-dimensional travel time

(taur=tau/tr) through the hyporheic zone.

```
Clear[kO2Satvar, kNO3Satvar, kO2Inhvar, deltavar, alphavar,
  betavar, kappavar, cO2, cNH4, cNO3, cNO3N, cN2N, cN2, solnnoAM, end];
solnnoAM[kO2Satvar_, kNO3Satvar_, kO2Inhvar_, deltavar_,
   alphavar_, betavar_, kappavar_, tr_] :=
  NDSolve[{(1 / 2.303) cO2'[u] == (10^u) (-Exp[-((qH0 * tr * 10^u) / (theta * z0))^2]
         (cO2[u] / (cO2[u] / kO2Satvar + 1)) - 2 deltavar cO2[u] cNH4[u]),
    cO2[-10] == 1, (1 / 2.303) cNH4'[u] == (10^u) ( -deltavar cO2[u] cNH4[u]),
    cNH4[-10] == alphavar, (1 / 2.303) cNO3'[u] ==
     (10^u) (-Exp[-((qH0 * tr * 10^u) / (theta * z0))^2] kappavar kO2Satvar kO2Inhvar
        cNO3[u]  / ((cO2[u] + kO2Inhvar) (cNO3[u] + cNO3N[u] + kNO3Satvar ))),
    cNO3[-10] == betavar, (1 / 2.303) cNO3N'[u] == (10^u) (deltavar cO2[u] cNH4[u] -
        Exp[-((qH0 * tr * 10^u) / (theta * z0))^2] kappavar kO2Satvar kO2Inhvar
         cNO3N[u]  / ((cO2[u] + kO2Inhvar) (cNO3[u] + cNO3N[u] + kNO3Satvar ))),
    cNO3N[-10] == 0, (1 / 2.303) cN2N'[u] == (10^u)
      ((1 / 2) Exp[-((qH0 * tr * 10^u) / (theta * z0))^2] kappavar kO2Satvar kO2Inhvar
        cNO3N[u]  / ((cO2[u] + kO2Inhvar) (cNO3[u] + cNO3N[u] + kNO3Satvar ))),
    cN2N[-10] == 0, (1 / 2.303) cN2'[u] == (10^u)
      ((1 / 2) Exp[-((qH0 * tr * 10^u) / (theta * z0))^2] kappavar kO2Satvar kO2Inhvar
        cNO3[u]  / ((cO2[u] + kO2Inhvar) (cNO3[u] + cNO3N[u] + kNO3Satvar ))),
    cN2[-10] == 0, WhenEvent[cO2[u] < 10^-5, cO2[u] → 0],
    WhenEvent[cNH4[u] < 10^-5, cNH4[u] → 0],
    WhenEvent[(cNO3[u] + cNO3N[u]) / beta < 10^-5, {end = u, "StopIntegration"}]},
   {cO2, cNH4, cNO3, cNO3N, cN2N, cN2}, {u, -10, 10}];
```

Step 3: Plot the concentration profiles versus non–dimensional (tau/tr) travel time through the hyporheic zone.

```
Clear[snnoAM];
snnoAM = solnnoAM[kO2SatHat, kNO3SatHat, kO2InhHat, delta, alpha, beta, kappa, tr];
LogPlot[{cO2[u] /. snnoAM, (cNH4[u] / alpha) /. snnoAM,
  (cNO3[u] + cNO3N[u]) / beta /. snnoAM}, {u, -3, 10}, PlotRange → {.00001, 10},
 AxesLabel → {"log10(tau/tr)", "C_HZ/C_Stream"}, PlotStyle → {Blue, Orange, Green},
 PlotLabels → Placed[{"oxygen", "ammonium", "nitrate"}, {Scaled[1], Before}]]
```

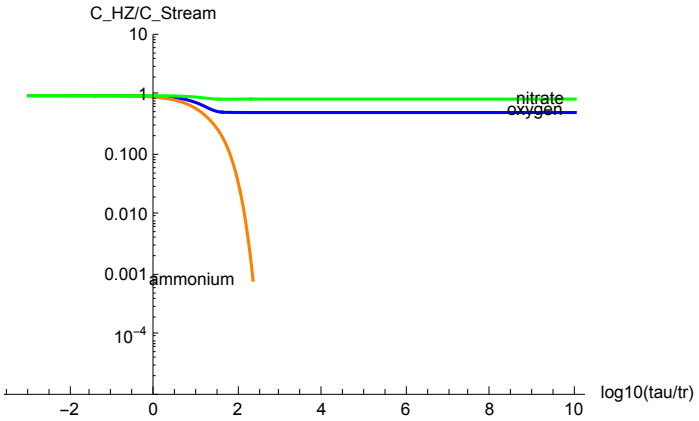

Step 4: Calculate direct denitrification uptake velocity (m/s).

```
vfden = 2 * ((qH0 / beta) * (NIntegrate[(cN2[u + Log10[tT / tr]] /. snnoAM)
        (frtdupmax PDF[𝒟up, u] + frtddnmax PDF[𝒟dn, u]),
      {u, -10 - Log10[tT / tr], 10 - Log10[tT / tr]}, WorkingPrecision → 10]))
```

In[1]:=
```
Export["vfden.pdf", EvaluationNotebook[]]
```

Out[1]= vfden.pdf